TABLE 2
Continued

[a] Trisomy of chromosome 4.
[b] Trisomy of chromosome 10.
[c] The number of genes involved in the aberration was counted as 'known genes' in UCSC Genome Browser.
[d] M1113-2 has a mutation of 8-bp deletion of *p16Ink4a*.
ND; no aberration detected.
* Fisher's exact probability test.
† Mann-Whitney *U* test.

Quantitative RT-PCR

The expression of *Gapdh* was used as a real-time PCR internal standard (TaqMan Rodent GAPDH Control Reagent, VIC Probe; Applied Biosystems) and was measured according to the manufacturer's instructions. The reaction was performed using an Mx3000P real-time PCR system (Stratagene, La Jolla, CA). The cDNA concentrations of the samples were adjusted so that the fluctuation of *Gapdh* expression was less than twofold among samples. Then qPCR analysis of the genes of interest was performed using a commercial mixture of Taq DNA polymerase and a fluorescent dye (SYBR Green Premix Ex Taq; Takara Bio Inc., Otsu, Japan). The PCR program consisted of a denaturation step at 95°C for 10 s, followed by 45 cycles at 95°C for 5 s and 60°C for 20 s. The primer sequences are listed in Table 1. Relative gene expression was calculated using the $2^{-\Delta\Delta Ct}$ method (*21*).

Western Blotting

Total crude protein was extracted by dissolving previously frozen tumor tissue samples in ice-cold lysis buffer (Invitrogen, no. 9803) that contained 1 m*M* phenylmethylsulfonyl fluoride for 30 min, homogenizing the ice-cold samples (MixerMill MM-300; Qiagen) twice for 20 s, and sonicating the samples five times for 30 s. Protein concentrations were quantified using the bicinchonic acid method (BCA™ Protein Assay kit; Pierce, Rockford, IL). The proteins of the crude lysates (50 μg) were separated using sodium dodecyl sulfate polyacrylamide gel electrophoresis and transferred onto polyvinylidene fluoride membranes (Millipore, Bedford, MA). The membranes were probed with goat polyclonal anti-p15Ink4b (M-20, sc-1429, Santa Cruz Biotechnology, Santa Cruz, CA), mouse monoclonal anti-p16Ink4a (F-12, sc-1661, Santa Cruz Biotechnology), goat polyclonal anti-p19Arf (G-19, sc-7403, Santa Cruz Biotechnology), anti-Rb (Ab-6) Mouse mAb (AF11) (OP77, Calbiochem, San Diego, CA), and goat polyclonal anti-actin (I-19, sc-1616, Santa Cruz Biotechnology) in 10 m*M* Tris-HCl (pH 7.4), 0.1 *M* NaCl, 0.1% Tween-20 and 5% bovine serum albumin. The antibodies were detected using peroxidase-conjugated anti-mouse or anti-goat IgG antibodies (ECL Plus Western Blotting Detection Reagents; GE Healthcare, Piscataway, NJ).

Immunohistochemistry

Immunohistochemistry was performed using an antibody against p16Ink4a (2D9A12, ab54210, Abcam, Cambridge, UK) as follows. Rehydrated specimens were prepared for antigen retrieval by first autoclaving them at 120°C for 20 min in 10 m*M* sodium citrate buffer (pH 6.0). To destroy endogenous peroxidase, samples were submerged in 0.3% hydrogen peroxide/methanol for 15 min. Nonspecific binding was blocked using a mixture of 10% normal goat serum (Cedarlane Laboratories, Ontario, Canada) and Protein Block serum-free protein in PBS, 0.015 *M* sodium azide (Dako, Carpenteria, CA). The specimens were incubated at 4°C overnight with anti-p16Ink4a (diluted 1:200), washed and then incubated with a peroxidase-conjugated secondary antibody [Histofine Simple Stain MAX PO(M) kit, Nichirei Biosciences, Tokyo, Japan]. Peroxidase activity was visualized by staining with diaminobenzidine (Simple Stain DAB Solution; Nichirei Biosciences). After counterstaining with hematoxylin, the specimens were dehydrated, mounted and examined.

RESULTS

Trisomies of Chromosome 4, Amplification of Chromosomal Region 1q12 and Deletions of Chromosomal Regions 3q35q36, 5q32 and 7q11 in the Genomes of Radiation-Induced Rat Mammary Carcinomas

We first looked for DNA copy number aberrations in 21 rat mammary carcinomas (seven of which had been induced by irradiation at 3 weeks of age, another seven of which had been induced by irradiation at 7 weeks of age, and seven that had developed spontaneously) using CGH microarrays with an average resolution of 19.1 kb. Table 2 lists the aberrations found that involved more than 10 probes with sequences aligned consecutively in the genome. The chromosomes of 14 carcinomas contained a total of 28 aberrations, whereas those of the other seven carcinomas did not meet the criterion of an aberration involving more than 10 probes. Twelve aberrations were associated with six of the seven carcinomas induced by irradiation at 3 weeks of age, 14 aberrations were associated with six of the seven carcinomas induced by irradiation at 7 weeks of age, and two aberrations were associated with two of the seven carcinomas that developed spontaneously in untreated rats (Table 2). Thus the fraction of radiation-induced carcinoma having any form of aberration or deletion was significantly higher than that of the spontaneous ones (Table 2D).

However, the aberrations did not converge upon any specific chromosomal regions so as to allow identification of causal genetic alterations. Ten of the 28 aberrations were located within regions where specific genes have not yet been assigned. Trisomies of chromosome 4 and 10 were found for three and one radiation-induced carcinomas, respectively (Fig. 1C for chromosome 4). Two carcinomas induced by irradiation at 7 weeks of age each had a deletion in the chromosomal region 3q35q36 (1.6 and 17.4 Mb in length) (Fig. 1B). The average $\log_2$ ratio of DNA copy numbers of carcinoma to that of corresponding normal tissue was −0.66 and −0.14 (which are calculated to be 0.6- and 0.9-fold of normal tissue, respectively) for the two deletions. Two carcinomas induced by irradiation at 3 weeks of age had deletions in the chromosomal region 5q32 (0.4 Mb in length; Fig. 1D), for which all of the *p16Ink4a*, *p19Arf* (encoded by the cyclin-dependent kinase [cdk] inhibitor gene, *Cdkn2a*), and *p15Ink4b* (encoded by

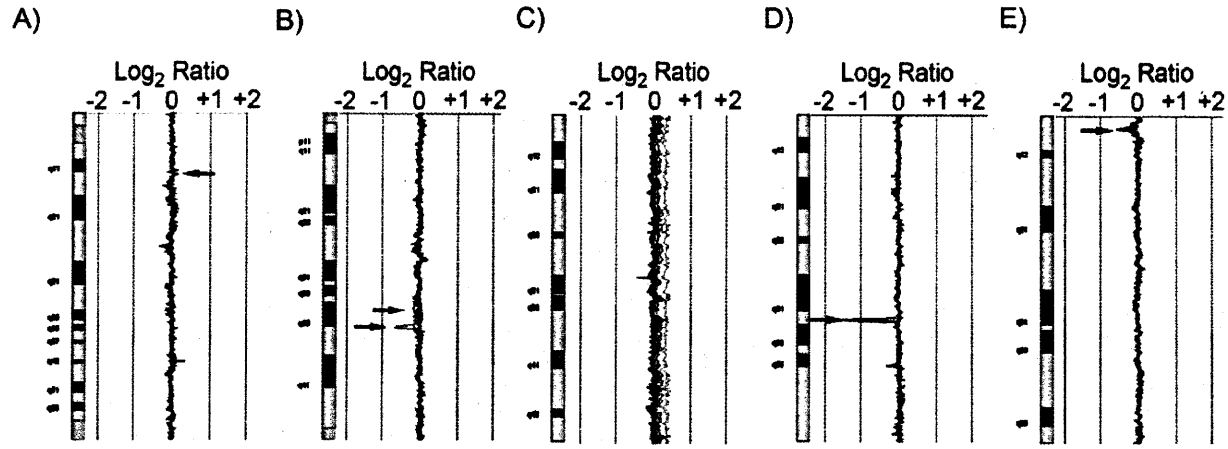

FIG. 1. Results of array CGH analyses. Each panel (A, chromosome 1; B, chromosome 3; C, chromosome 4; D, chromosome 5; E, chromosome 7) shows the merged results for the chromosomes of the 14 radiation-induced carcinomas and seven spontaneous carcinomas. Arrows indicate the positions of the aberrations. Amplifications of interstitial genomic region of chromosome 1 and whole chromosome 4 for two and three carcinomas are shown in panels A and C, respectively, and deletions at interstitial genomic regions of chromosomes 3, 5 and 7 in two, two and four carcinomas are shown in panels B, D and E, respectively.

Cdkn2b) exons and some of the *Mtap* exons were lost. The average $\log_2$ ratios of DNA copy numbers in these two carcinomas were −2.43 and −0.81 (calculated to be changes of 0.2- and 0.6-fold), respectively, strongly indicating the occurrence of homozygous and hemizygous deletions, respectively. Carcinomas induced by irradiation at 3 or 7 weeks of age had an amplification and a deletion of the chromosomal regions 1q12 and 7q11 (Fig. 1A and 1E) in two and four carcinomas, respectively; to date, however, no genes have been assigned to these regions (Table 2). No other aberrations were found in the chromosomes of more than one carcinoma. The chromosomes of spontaneous mammary carcinomas contained two aberrations for which there were amplifications of the chromosomal region 2q44q45, which contains 30 genes, and 10q31, which contains *Neurod2* (neurogenic differentiation 2), *Ppp1r1b* (protein phosphatase 1, regulatory [inhibitor] subunit 1B), *Erbb2* (v-erb-b2 erythroblastic leukemia viral oncogene), and *Grb7* (growth factor receptor bound protein 7) (Table 2).

The Expression of p16Ink4a, p19Arf, and Rb is Abnormally Regulated in Radiation-Induced Mammary Carcinomas

It is well established that *CDKN2A* and *CDKN2B* are often deleted in various types of human tumors, and their transcription is down-regulated by hypermethylation of the CpG island in each gene's promoter region (*22, 23*). Therefore, we used quantitative PCR to examine the expression of *p15Ink4b*, *p16Ink4a* and *p19Arf* in radiation-induced rat mammary carcinomas. *p16Ink4a* and *p19Arf* were unexpectedly up-regulated for all carcinoma samples except one (M1493-1), which had a homozygous deletion at the *Cdkn2a/Cdkn2b* loci (Fig. 2A). The expression of *p16Ink4a* was also up-regulated in all of the spontaneous mammary carcinomas (data not shown). Because DNA methylation of the DNA in the promoter region is an important mechanism for the regulation of *p16Ink4a* expression (*24, 25*), we analyzed the methylation status of the *p16Ink4a* promoter region of these mammary carcinomas by bisulfite sequencing; however, the methylation status of all CpG sites was virtually unchanged (Fig. 2B). The *p15Ink4b* promoters of normal mammary tissues and mammary cancers were not methylated (data not shown). Because inactivating mutations of *p16Ink4a* may cause the up-regulation of p16Ink4a through a negative feedback loop, we sequenced the cDNAs of *p15Ink4b*, *p16Ink4a* and *p19Arf* obtained from mammary carcinomas and normal mammary tissues to identify possible point mutations. No point mutations were found, but a novel 8-bp deletion in the *p16Ink4a* sequence was identified [Fig. 2C (i)]. Additionally, for five of the eight carcinomas, we found a change of sequence in *p16Ink4a* that resulted in a phenylalanine replacing a leucine at position 151 (Leu151Phe), but this was judged to be a single nucleotide polymorphism because the same change was observed in normal tissues from corresponding rats [Fig. 2C (ii)]. We did not observe any meaningful changes in the sequences of *p15Ink4b* and *p19ARF* (data not shown). In all cases, the expression of p15Ink4b, p16Ink4a and p19Arf proteins was increased compared with normal mammary tissue (Fig. 2D). Interestingly, p16Ink4a expression was observed in two carcinoma samples (M1493-1 and M1501-2) for which *Cdkn2a* and *Cdkn2b* had been deleted, suggesting that normal cells contaminated the carcinoma samples. This possibility led us to investigate the cellular locations of the proteins using immunohistochemistry. As shown in Fig. 3A, for normal mammary tissue, p16Ink4a was found in epithelial cells. For

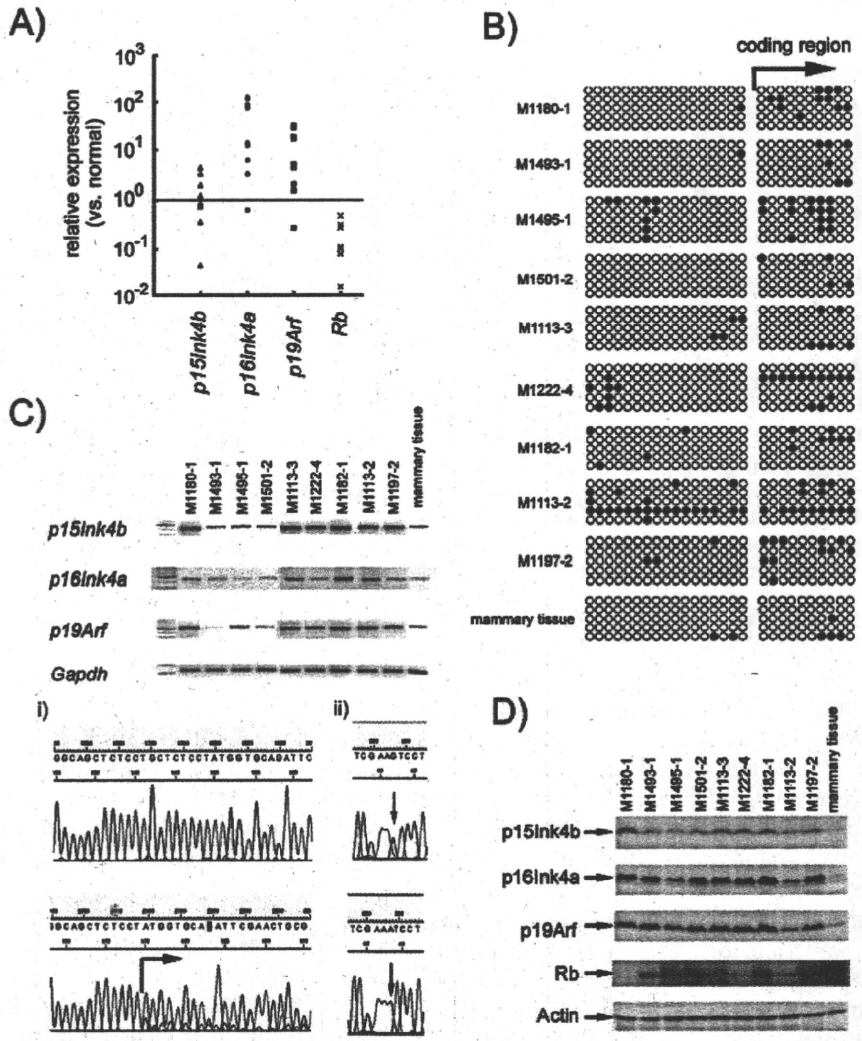

FIG. 2. Aberrant expression of the p16Ink4a/Rb pathway components. Panel A: Quantitative PCR characterization of the expression of *p15Ink4b*, *p16Ink4a*, *p19Arf* and *Rb* using primers specific for each gene. Relative gene expression was calculated in comparison with that of normal mammary tissue. Each symbol represents one tumor sample. Panel B: The CpG island methylation status of 27 CpG dinucleotides in the promoter region of *p16Ink4a*. Each circle represents a CpG site in the genomic DNA sequence, and each row of circles represents the analysis of a single cloned allele. Closed circles, methylated CpG dinucleotides; open circles, unmethylated CpG dinucleotides. Panel C: RT-PCR analysis of *p15Ink4b*, *p16Ink4a*, *p19Arf* and *Gapdh* using primers specific for each gene. i): Sequence of p16Ink4a genes isolated from radiation-induced mammary carcinomas. Shown are sequencing data of wild-type *p16Ink4a* (upper panel) and that of a mutated sequence containing an 8-bp deletion (M1113-2, lower panel). The black arrow indicates the start of the deletion site. ii): The single nucleotide polymorphism (CTT to TTT) found in *p16Ink4a* at codon 151, which changes a leucine to a phenylalanine. Sequencing of *p16Ink4a* of two carcinomas (AAG in upper panel, AAA in lower panel; read on the reverse strand). Panel D: Western blot analysis of expressed p15Ink4b, p16Ink4a, p19Arf and Rb stained with their corresponding antibodies. Actin, included in each sample, served as an internal standard.

mammary carcinomas harboring both *Cdkn2a* and *Cdkn2b*, p16Ink4a was observed in both epithelial cells and stromal fibroblastic cells (Fig. 3B and D). For carcinoma in which *p16Ink4a* had been deleted from genomes (M1493-1 and M1501-2), p16Ink4a was absent (Fig. 3C) in all but a small number of regions. No correlation was found between the expression levels of p16Ink4a protein and mRNA (Fig. 2C and D).

It has been reported that some breast cancers have increased expression of *p16INK4A* in comparison with normal mammary tissues and that the increase correlates with malignant phenotypes (*26, 27*). Additionally, the expression of *p16INK4A* inversely correlates with the expression of the Rb protein (*26, 28, 29*). We therefore examined the expressions of Rb mRNA and protein and found that these expressions were down-regulated in the

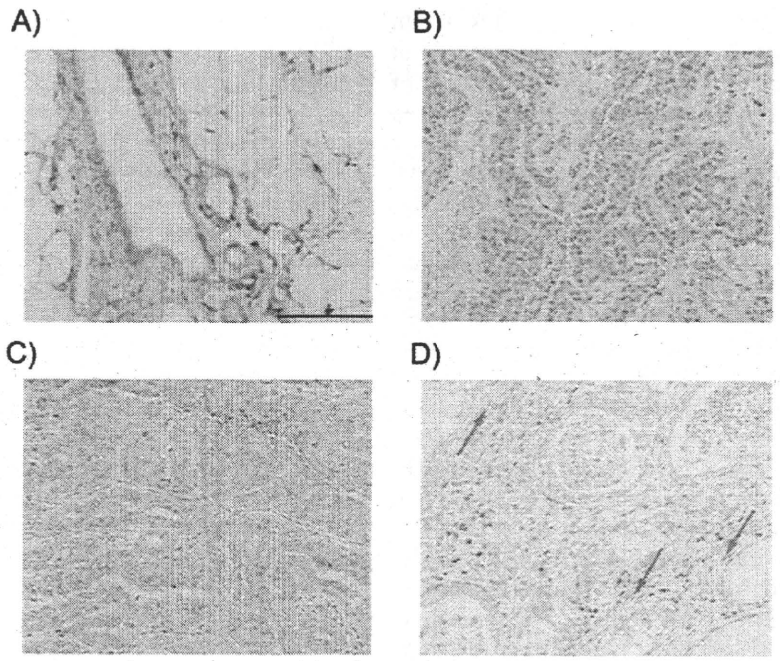

FIG. 3. Immunohistochemical staining for p16Ink4a. Panel A: Normal mammary tissue. Panel B: A p16Ink4a-positive mammary carcinoma tissue. Panel C: The tissue of a mammary carcinoma containing a homozygous deletion of the chromosomal region 5q32. Panel D: The tissue of a mammary carcinoma showing stromal staining (red arrows). Bar, 200 μm.

mammary carcinomas compared with normal mammary tissue (Fig. 2A and D).

DISCUSSION

In the current study, copy number aberrations associated with the chromosomes of spontaneous and radiation-induced rat mammary carcinomas were detected using array CGH analysis. We found an increase in the number of copies of chromosome 4 (trisomy), an amplification of the chromosomal region 1q12, and deletions in the chromosomal regions 3q35q36, 5q32 and 7q11 in more than one mammary carcinoma. However, we did not observe any specific gene that showed aberrations in the majority of carcinomas, which is in contrast with previous reports on radiation-induced carcinomas (*6, 7, 10*). Nevertheless, we found that the majority of radiation-induced carcinomas, but not spontaneous ones, had some form of DNA copy number aberration, illustrating the association between copy number aberrations and radiation-induced rat mammary carcinoma.

There have been a number of reports of genomic alterations associated with rat mammary carcinomas that were found using conventional (non-array-based) CGH. The genomes of rat mammary carcinomas induced by 2-amino-1-methyl-6-phenylimidazo[4,5-b]-pyridine (PhIP) were shown to have often lost parts of chromosomes 2, 3, 11, 18 and X and to have regions of chromosomes 1, 7 and 10 amplified. For carcinomas induced by 7,12-dimethylbenz[a]anthracene (DMBA), chromosomes showed no consistent pattern of deletion or amplification (*30*). High-resolution oligonucleotide array CGH (5.3 kb) failed to detect gross chromosomal changes in DMBA-induced rat mammary carcinomas (*31*). Nonrandom amplifications of regions of chromosomes 1, 4, 7, 9, 11, 13 and 20 have been reported for the genomes of 17β-estradiol-induced mammary carcinomas of ACI rats (*32*). We found that changes in the genomes of radiation-induced mammary carcinomas included the gain of the chromosomal region 1q12, the loss of the chromosomal regions 3q35q36, 5q32 and 7q11 and trisomy of chromosome 4, and, for a spontaneous mammary carcinoma, amplification of the chromosomal regions 2q44q45 and 10q31. In particular, the chromosomal region 10q31 includes *Erbb2*, which is commonly amplified in PhIP-induced carcinomas (*30*).

In our present study, chromosomal region 3q35q36 was deleted in two radiation-induced mammary carcinomas. This region contains seven genes: *Myef2* (myelin basic protein expression factor 2, repressor), *Slc12a1* (solute carrier family 12 [sodium/potassium/chloride transporters] member 1), *Rpl32* (ribosomal protein L32), *Dut* (deoxyuridine triphosphatase), *Fbn1* (fibrillin 1), *Cops2* (COP9 constitutive photomorphogenic homolog subunit 2), and *Galk2* (galactokinase 2). Specifically, *Fbn1* is putatively associated with human primary breast cancer (*33*). Therefore, deletion of the chromosomal region 3q35q36 may be causatively associated with radiation-induced mammary carcinogenesis. We also observed the amplification and deletion of chromosomal regions 1q12 and 7q11 in two and four radiation-induced mammary carcinomas, respectively; however, genes have not yet

been assigned to these chromosomal regions. The deletion of chromosomal region 7q11 has also been observed in PhIP-induced mammary carcinoma (*30*). Trisomy of chromosome 4, which we observed here, has not been found in mammary carcinomas induced by DMBA or PhIP (*30, 31*). However, it has been observed in many cell lines derived from neurogenic carcinomas induced in rats by ethylnitrosourea (*34*). Partial amplifications of chromosome 4 have also been observed in rat sarcomas induced by DMBA, suggesting that amplification of the *Met* proto-oncogene may be important (*35*). The trisomy of chromosome 4 and the deletion of chromosomal region 7q11 may thus be functionally significant during tumorigenesis in rats even though these events occur independently of tissue and carcinogen type.

The $\log_2$ ratio of the aberrations detected in our study varied between carcinomas, indicating that these tumors have different amounts of contaminating normal cells. By mixing normal genomic DNA with target samples, Hodgson *et al.* (*36*) have showed that normal cells influence the ability to detect single-copy number changes. Their study has indicated that single-copy gains and losses can be detected reliably in samples in which as little as 40% of the DNA is from the tumor. This sensitivity allows detection of copy number aberrations in tumors containing substantial stromal components that cannot be removed and/or detection of aberrations present in only a fraction of tumor cells.

Deletion of the chromosome 5q32 region in two of the radiation-induced carcinomas strongly indicates a causative role for *Cdkn2a*/*Cdkn2b* inactivation during carcinogenesis. This region contains four genes: *p15Ink4b*, *p16Ink4a* (encoding two cdk inhibitors), *p19Arf* and *Mtap* (methylthioadenosine phosphorylase). The binding of p16Ink4a or p15Ink4b to Cdk4 or Cdk6 induces an allosteric change that abrogates the binding of these kinases to cyclin D1 and consequently inhibits Cdk4/6-mediated phosphorylation of Rb. Thus expression of p15Ink4b and p16Ink4a maintains Rb in a hypophosphorylated/activated state, so that the binding of Rb to transcription factor E2F causes G_1 cell cycle arrest. As mentioned above, it is well established that CDKN2A and CDKN2B are often deleted in various types of human tumors; on the other hand, deletion of the chromosome 5q32 region was not observed in rat mammary tumors (*30–32*). In our present study, *p16Ink4a* expression was up-regulated in most of the radiation-induced carcinomas (*37*), but we could not clearly define the precise mechanisms underlying this *p16Ink4a* up-regulation. Because the transcription of *p16Ink4a* appears to be tightly regulated in a negative feedback loop mediated by Rb (*22, 38*), the observed up-regulated expression of p16Ink4a in rat mammary tumors may be a result of release from transcriptional repression by Rb. This speculation is in line with our observation that methylation of the *p16Ink4a* promoter, although being another effective way to regulate p16Ink4a expression (*24, 25*), did not correlate with p16Ink4a expression. Although there were some inconsistencies between the p16Ink4a mRNA and protein levels in our study (Fig. 2A and D), p16Ink4a level may be controlled post-transcriptionally, as has been reported for p16Ink4a of human Ewing's sarcoma and adult T-cell leukemia/lymphoma (*39, 40*). Moreover, the degree of stromal overexpression of p16INK4A in human breast phyllodes tumors has been found to correlate with the histological grade of the tumor (*41*), underscoring the importance of our finding that p16Ink4a is expressed in the stroma of rat mammary carcinomas.

In summary, the present study indicates, for the first time, that rat mammary carcinoma induced by radiation is characterized by frequent DNA copy number changes that do not converge on specific genes. Disruption of the p16Ink4a/Rb pathway was observed in all carcinomas, owing in part to deletion of 5q32.

ACKNOWLEDGMENTS

The authors thank M. Ootawara, H. Osada, N. Kowatari, H. Moritake, S. Sasaki, Y. Amasaki, M. Okabe and T. Honda for technical assistance, the Laboratory Animal Science Section, National Institute of Radiological Sciences, for animal management, and E. Obara, Y. Sugawara, F. Mizumoto and K. Hirasawa for secretarial help. This research was supported in part by a Grant-In-Aid for Young Scientists (B) from MEXT (No. 20710049), a research grant from the Takeda Science Foundation, a Long-Range Research Initiative grant from the Japan Chemical Industry Association (No. 2006CC03-01), the Third-Term Comprehensive Strategy for Cancer Control (No. 19141201), and a Grant-In-Aid for Cancer Research (No. 19S-1) from the Ministry of Health, Labor, and Welfare of Japan.

Received: September 11, 2009; accepted: March 26, 2010; published online: May 26, 2010

REFERENCES

1. J. B. Little, Radiation carcinogenesis. *Carcinogenesis* **21**, 397–404 (2000).
2. D. L. Preston, E. Ron, S. Tokuoka, S. Funamoto, N. Nishi, M. Soda, K. Mabuchi and K. Kodama, Solid cancer incidence in atomic bomb survivors: 1958–1998. *Radiat. Res.* **168**, 1–64 (2007).
3. L. Huang, A. R. Snyder and W. F. Morgan, Radiation-induced genomic instability and its implications for radiation carcinogenesis. *Oncogene* **22**, 5848–5854 (2003).
4. S. Kakinuma, M. Nishimura, S. Sasanuma, K. Mita, G. Suzuki, Y. Katsura, T. Sado and Y. Shimada, Spectrum of Znfn1a1 (Ikaros) inactivation and its association with loss of heterozygosity in radiogenic T-cell lymphomas in susceptible B6C3F1 mice. *Radiat. Res.* **157**, 331–340 (2002).
5. M. Nakashima, N. Takamura, H. Namba, V. Saenko, S. Meirmanov, N. Matsumoto, T. Hayashi, S. Maeda and I. Sekine, RET oncogene amplification in thyroid cancer: correlations with radiation-associated and high-grade malignancy. *Hum. Pathol.* **38**, 621–628 (2007).

6. Y. Wakabayashi, J. Inoue, Y. Takahashi, A. Matsuki, H. Kosugi-Okano, T. Shinbo, Y. Mishima, O. Niwa and R. Kominami, Homozygous deletions and point mutations of the Rit1/Bcl11b gene in gamma-ray induced mouse thymic lymphomas. *Biochem. Biophys. Res. Commun.* **301**, 598–603 (2003).
7. Y. Shimada, M. Nishimura, S. Kakinuma, M. Okumoto, T. Shiroishi, K. H. Clifton and S. Wakana, Radiation-associated loss of heterozygosity at the Znfn1a1 (Ikaros) locus on chromosome 11 in murine thymic lymphomas. *Radiat. Res.* **154**, 293–300 (2000).
8. T. Paunesku, Y. Zhang, M. A. Gemmell and G. E. Woloschak, p53 gene deletions in paraffin-preserved lymphoid tumors from irradiated mice. *Leuk. Res.* **24**, 511–517 (2000).
9. C. W. Miller, A. Aslo, C. Tsay, D. Slamon, K. Ishizaki, J. Toguchida, T. Yamamuro, B. Lampkin and H. P. Koeffler, Frequency and structure of p53 rearrangements in human osteosarcoma. *Cancer Res.* **50**, 7950–7954 (1990).
10. S. Miura, M. Nakashima, M. Ito, H. Kondo, S. Meirmanov, T. Hayashi, M. Soda, T. Matsuo and I. Sekine, Significance of HER2 and C-MYC oncogene amplifications in breast cancer in atomic bomb survivors: associations with radiation exposure and histologic grade. *Cancer* **112**, 2143–2151 (2008).
11. E. H. van Beers and P. M. Nederlof, Array-CGH and breast cancer. *Breast Cancer Res.* **8**, 210 (2006).
12. J. Climent, J. L. Garcia, J. H. Mao, J. Arsuaga and J. Perez-Losada, Characterization of breast cancer by array comparative genomic hybridization. *Biochem. Cell Biol.* **85**, 497–508 (2007).
13. K. Unger, E. Malisch, G. Thomas, H. Braselmann, A. Walch, G. Jackl, P. Lewis, E. Lengfelder, T. Bogdanova and H. Zitzelsberger, Array CGH demonstrates characteristic aberration signatures in human papillary thyroid carcinomas governed by RET/PTC. *Oncogene* **27**, 4592–4602 (2008).
14. S. Nandi, R. C. Guzman and J. Yang, Hormones and mammary carcinogenesis in mice, rats, and humans: a unifying hypothesis. *Proc. Natl. Acad. Sci. USA* **92**, 3650–3657 (1995).
15. T. Imaoka, M. Nishimura, D. Iizuka, K. Daino, T. Takabatake, M. Okamoto, S. Kakinuma and Y. Shimada, Radiation-induced mammary carcinogenesis in rodent models: what's different from chemical carcinogenesis? *J. Radiat. Res. (Tokyo)* **50**, 281–293 (2009).
16. T. Imaoka, M. Nishimura, S. Kakinuma, Y. Hatano, Y. Ohmachi, S. Yoshinaga, A. Kawano, A. Maekawa and Y. Shimada, High relative biologic effectiveness of carbon ion radiation on induction of rat mammary carcinoma and its lack of H-ras and Tp53 mutations. *Int. J. Radiat. Oncol. Biol. Phys.* **69**, 194–203 (2007).
17. T. Imaoka, M. Nishimura, Y. Nishimura, S. Kakinuma and Y. Shimada, Persistent cell proliferation of terminal end buds precedes radiation-induced rat mammary carcinogenesis. *In Vivo* **20**, 353–358 (2006).
18. T. Imaoka, M. Nishimura, A. Teramoto, Y. Nishimura, M. Ootawara, H. Osada, S. Kakinuma, A. Maekawa and Y. Shimada, Cooperative induction of rat mammary cancer by radiation and 1-methyl-1-nitrosourea via the oncogenic pathways involving c-Myc activation and H-ras mutation. *Int. J. Cancer* **115**, 187–193 (2005).
19. T. Imaoka, S. Yamashita, M. Nishimura, S. Kakinuma, T. Ushijima and Y. Shimada, Gene expression profiling distinguishes between spontaneous and radiation-induced rat mammary carcinomas. *J. Radiat. Res. (Tokyo)* **49**, 349–360 (2008).
20. J. D. Haag, L. C. Hsu, M. A. Newton and M. N. Gould, Allelic imbalance in mammary carcinomas induced by either 7,12-dimethylbenz[a]anthracene or ionizing radiation in rats carrying genes conferring differential susceptibilities to mammary carcinogenesis. *Mol. Carcinog.* **17**, 134–143 (1996).
21. K. J. Livak and T. D. Schmittgen, Analysis of relative gene expression data using real-time quantitative PCR and the 2(–Delta Delta C(T)) method. *Methods* **25**, 402–408 (2001).
22. A. Okamoto, D. J. Demetrick, E. A. Spillare, K. Hagiwara, S. P. Hussain, W. P. Bennett, K. Forrester, B. Gerwin, M. Serrano and D. H. Beach, Mutations and altered expression of p16INK4 in human cancer. *Proc. Natl. Acad. Sci. USA* **91**, 11045–11049 (1994).
23. J. G. Herman, J. Jen, A. Merlo and S. B. Baylin, Hypermethylation-associated inactivation indicates a tumor suppressor role for p15INK4B. *Cancer Res.* **56**, 722–727 (1996).
24. M. Abe, E. Okochi, T. Kuramoto, A. Kaneda, T. Takato, T. Sugimura and T. Ushijima, Cloning of the 5′ upstream region of the rat p16 gene and its role in silencing. *Jpn. J. Cancer Res.* **93**, 1100–1106 (2002).
25. K. Honoki, T. Tsujiuchi, T. Mori, K. Yoshitani, M. Tsutsumi, Y. Takakura and Y. Mii, Expression of the p16INK4a gene and methylation pattern of CpG sites in the promoter region in rat tumor cell lines. *Mol. Carcinog.* **39**, 10–14 (2004).
26. K. Milde-Langosch, A. M. Bamberger, G. Rieck, B. Kelp and T. Loning, Overexpression of the p16 cell cycle inhibitor in breast cancer is associated with a more malignant phenotype. *Breast Cancer Res. Treat.* **67**, 61–70 (2001).
27. S. C. Wong, J. K. Chan, K. C. Lee and W. L. Hsiao, Differential expression of p16/p21/p27 and cyclin D1/D3, and their relationships to cell proliferation, apoptosis, and tumour progression in invasive ductal carcinoma of the breast. *J. Pathol.* **194**, 35–42 (2001).
28. E. A. Dublin, N. K. Patel, C. E. Gillett, P. Smith, G. Peters and D. M. Barnes, Retinoblastoma and p16 proteins in mammary carcinoma: their relationship to cyclin D1 and histopathological parameters. *Int. J. Cancer* **79**, 71–75 (1998).
29. V. G. Gorgoulis, E. N. Koutroumbi, A. Kotsinas, P. Zacharatos, C. Markopoulos, L. Giannikos, V. Kyriakou, Z. Voulgaris, I. Gogas and C. Kittas, Alterations of p16-pRb pathway and chromosome locus 9p21–22 in sporadic invasive breast carcinomas. *Mol. Med.* **4**, 807–822 (1998).
30. A. T. Christian, E. G. Snyderwine and J. D. Tucker, Comparative genomic hybridization analysis of PhIP-induced mammary carcinomas in rats reveals a cytogenetic signature. *Mutat. Res.* **506–507**, 113–119 (2002).
31. T. Adamovic, D. McAllister, V. Guryev, X. Wang, J. W. Andrae, E. Cuppen, H. J. Jacob and S. L. Sugg, Microalterations of inherently unstable genomic regions in rat mammary carcinomas as revealed by long oligonucleotide array-based comparative genomic hybridization. *Cancer Res.* **69**, 5159–5167 (2009).
32. J. J. Li, S. J. Weroha, W. L. Lingle, D. Papa, J. L. Salisbury and S. A. Li, Estrogen mediates Aurora-A overexpression, centrosome amplification, chromosomal instability, and breast cancer in female ACI rats. *Proc. Natl. Acad. Sci. USA* **101**, 18123–18128 (2004).
33. W. Chen, M. Salto-Tellez, N. Palanisamy, K. Ganesan, Q. Hou, L. K. Tan, L. H. Sii, K. Ito, B. Tan and P. Tan, Targets of genome copy number reduction in primary breast cancers identified by integrative genomics. *Genes Chromosomes Cancer* **46**, 288–301 (2007).
34. W. Au, S. W. Soukup and T. I. Mandybur, Excess chromosome no. 4 in ethylnitrosourea-induced neurogenic tumor lines of the rat. *J. Natl. Cancer Inst.* **59**, 1709–1716 (1977).
35. A. Walentinsson, A. Sjoling, K. Helou, K. Klinga-Levan and G. Levan, Genomewide assessment of genetic alterations in DMBA-induced rat sarcomas: cytogenetic, CGH, and allelotype analyses reveal recurrent DNA copy number changes in rat chromosomes 1, 2, 4, and 7. *Genes Chromosomes Cancer* **28**, 184–195 (2000).
36. G. Hodgson, J. H. Hager, S. Volik, S. Hariono, M. Wernick, D. Moore, N. Nowak, D. G. Albertson, D. Pinkel and J. W. Gray, Genome scanning with array CGH delineates regional alterations in mouse islet carcinomas. *Nat. Genet.* **29**, 459–464 (2001).
37. J. Silva, J. M. Silva, G. Dominguez, J. M. Garcia, B. Cantos, R. Rodriguez, F. J. Larrondo, M. Provencio, P. Espana and F. Bonilla, Concomitant expression of p16INK4a and p14ARF in

primary breast cancer and analysis of inactivation mechanisms. *J. Pathol.* **199**, 289–297 (2003).

38. Y. Li, M. A. Nichols, J. W. Shay and Y. Xiong, Transcriptional repression of the D-type cyclin-dependent kinase inhibitor p16 by the retinoblastoma susceptibility gene product pRb. *Cancer Res.* **54**, 6078–6082 (1994).

39. Y. Takasaki, Y. Yamada, K. Sugahara, T. Hayashi, N. Dateki, H. Harasawa, S. Kawabata, H. Soda, S. Ikeda and S. Kamihira, Interruption of p16 gene expression in adult T-cell leukaemia/lymphoma: clinical correlation. *Br. J. Haematol.* **122**, 253–259 (2003).

40. S. C. Brownhill, C. Taylor and S. A. Burchill, Chromosome 9p21 gene copy number and prognostic significance of p16 in ESFT. *Br. J. Cancer* **96**, 1914–1923 (2007).

41. A. Kuijper, R. A. de Vos, J. H. Lagendijk, E. van der Wall and P. J. van Diest, Progressive deregulation of the cell cycle with higher tumor grade in the stroma of breast phyllodes tumors. *Am. J. Clin. Pathol.* **123**, 690–698 (2005).

Mutation Research 686 (2010) 30–38

Contents lists available at ScienceDirect

Mutation Research/Fundamental and Molecular Mechanisms of Mutagenesis

journal homepage: www.elsevier.com/locate/molmut
Community address: www.elsevier.com/locate/mutres

Complicated biallelic inactivation of *Pten* in radiation-induced mouse thymic lymphomas

Yu Yamaguchi[a,b,1,2], Takashi Takabatake[b,1], Shizuko Kakinuma[b], Yoshiko Amasaki[b], Mayumi Nishimura[b], Tatsuhiko Imaoka[b], Kazumi Yamauchi[b], Yi Shang[b], Tomoko Miyoshi-Imamura[b,c], Hiroyuki Nogawa[a], Yoshiro Kobayashi[d], Yoshiya Shimada[b,*]

[a] *Department of Biology, Graduate School of Science, Chiba University, Yayoicho, Inage-ku, Chiba 263-8522, Japan*
[b] *Experimental Radiobiology for Children's Health Research Group, Research Center for Radiation Protection, National Institute of Radiological Sciences, 4-9-1, Anagawa, Inage-ku, Chiba 263-8555, Japan*
[c] *Genetic Counseling Program, Graduate School of Humanities and Sciences, Ochanomizu University, 2-1-1 Otsuka, Bunkyou-ku, Tokyo 112-8610, Japan*
[d] *Department of Biomolecular Science, Faculty of Science, Toho University, Miyama 2-2-1, Funabashi, Chiba 274-8510, Japan*

ARTICLE INFO

Article history:
Received 29 September 2009
Accepted 29 December 2009
Available online 7 January 2010

Keywords:
Pten
Thymic lymphoma
Epigenetic silencing
Mutation
Deletion
Radiation

ABSTRACT

Inactivation of the phosphatase and tensin homolog gene (*Pten*) occurs via multiple tissue-dependent mechanisms including epigenetic silencing, point mutations, insertions, and deletions. Although frequent loss of heterozygosity around the *Pten* locus and plausible involvement of epigenetic silencing have been reported in radiation-induced thymic lymphomas, the proportion of lymphomas with inactivated *Pten* and the spectrum of causal aberrations have not been extensively characterized. Here, we assessed the mode of *Pten* inactivation by comprehensive analysis of the expression and alteration of *Pten* in 23 radiation-induced thymic lymphomas developed in B6C3F1 mice. We found no evidence for methylation-associated silencing of *Pten*; rather, complex structural abnormalities comprised of missense and nonsense mutations, 1- and 3-bp insertions, and focal deletions were identified in 8 of 23 lymphomas (35%). Sequencing of deletion breakpoints suggested that aberrant V(D)J recombination and microhomology-mediated rearrangement were responsible for the focal deletions. Seven of the 8 lymphomas had biallelic alterations, and 4 of them did not express Pten protein. These *Pten* aberrations coincided with downstream Akt phosphorylation. In conclusion, we demonstrate that *Pten* inactivation is frequently biallelic and is caused by a variety of structural abnormalities (rather than by epigenetic silencing) and is involved in radiation-induced lymphomagenesis.

1. Introduction

The phosphatase and tensin homolog (Pten) is an important lipid phosphatase that antagonizes the phosphatidylinositol-3-kinase (PI3K)/Akt signaling pathway [1,2]. The PI3K/Akt signaling pathway is aberrantly activated in a variety of tumors, often resulting from defects in the *PTEN* gene [3,4]. Once activated, Akt promotes fundamental cellular processes such as cell survival, growth, proliferation, angiogenesis, and cellular metabolism. Pten also plays a crucial role as guardian of genome integrity by maintaining chromosomal stability through physical interaction with centromeres and by controlling DNA repair, both of which are independent of Akt activation [5].

PTEN is mutated in a variety of human carcinomas [6,7], and *PTEN* is the second most frequently mutated gene in human cancers after *TP53* [8,9]. Germline mutations of *PTEN* in humans are responsible for Cowden disease, which is characterized by a high risk for thyroid and breast cancers [10]. In addition to genetic alterations resulting in missense, nonsense or frameshift mutations, epigenetic silencing of *PTEN* has been reported in the pathogenesis of gastric and breast cancers [11,12]. Furthermore, overexpression of *PTEN*-targeting microRNAs correlates with decreased expression of PTEN protein in hepatocellular [13] and ovarian cancers [14]. These reports indicate that there are multiple mechanisms responsible for *PTEN* inactivation.

Interestingly, there are significant differences in the location of mutations in *PTEN* with respect to cancer type. For example, a high proportion of glioblastomas have missense mutations in exon 6, which encodes part of the phosphatase domain of PTEN, whereas few mutations have been found in exons 7 and 8, which encode

* Corresponding author. Tel.: +81 43 206 3200; fax: +81 43 206 4138.
E-mail address: y_shimad@nirsgo.jp (Y. Shimada).
[1] These authors contributed equally to this study.
[2] Present address: Pharmaceutical Research Laboratories, Sanwa Kagaku, Kenkyusho Co., Ltd., 363 Shiosaki, Hokusei-cho, Inabe-shi, Mie 511-0406, Japan.

0027-5107/$ – see front matter © 2010 Elsevier B.V. All rights reserved.
doi:10.1016/j.mrfmmm.2009.12.011

Table 1
Summary of expression and aberrations of Pten in 23 thymic lymphomas, in parallel with the activation of a downstream factor of Akt.

Tumor ID	LOH[a] status	Structural alteretations[b]	Transcriptional changes[b]	Predicted changes[c]	Pten protein	Akt protein[d]
TL5	–	Duplication of exon6 and exon7 509 Ins TGT	Additional faint long product nd	Ins of 103 amino acids 170S→ M and C	A faint larger band Low	Activated
TL14	C3H	Del of exon4 and exon5 9621ns A	Additional faint short product nd	Stop at codon264 Stop at codon333	Absent Absent	Activated
TL8	B6	Homozygous deletion	Absent	–	Absent	Activated
TL11	C3H	Homozygous deletion	Aberant splicing	Stop at codon54	Absent	Activated
TL20	B6	Homozygous deletion	Lack of sequence for exon 1	–	Absent	Activated
TL15	–	862 G→ G/T	nd	Stop codon	Low	Activated
TL19	C3H	158 T→ T/C[e]	nd	53 V→ A	Low	nd
TL21	C3H	364 A→ T	nd	122 I→ F	Low	Activated
TL12	C3H	nd	nd	–	Low	Activated
TL3	–	nd	nd	–	Low	nd
TL6	–	nd	nd	–	Low	nd

[a] Lost allele is shown. (–), retention of heterozygosity.
[b] Ins, insertion; Del, deletion; nd, not detected.
[c] S, serine; M, methionine; C, cysteine; V, valine; A, alanine; I, isoleucine; F, phenylalanine.
[d] "Activated" means that the phosphorylation of Akt protein at Ser473 was detected; nd, not detected.
[e] Sequencing analysis indicates the presence of both mutated and non-mutated sequence, the latter of which may be due to contaminated normal cells.

the C2 domain. In contrast, endometrial carcinomas rarely contain mutations in exon 6; rather, frameshift mutations in exons 7 and 8 are common [6,7]. Deletion of *PTEN* has been identified in 77% of prostate cancer cases, with 25% containing homozygous deletions [15]. Because previous studies have examined only single or limited categories of causal alterations, the overall contribution of each causal *PTEN* alteration remains unclear for many tumor types.

Radiation is a clear etiology for leukemia and lymphoma. Radiation-induced murine thymic lymphomas have been used as a suitable model of human T-cell acute lymphoblastic leukemia (ALL), many of which exhibit *Notch1* and *Ikaros* mutation, *p15* and *p16* alteration, and aberrant activation of Jak-Stat signaling [16–20]. Loss of heterozygosity (LOH) within a broad genomic region of chromosome 19, including the mouse *Pten* locus, has been demonstrated in many thymic lymphomas [21,22]. Although it has been suggested that *Pten* undergoes epigenetic silencing by DNA methylation in radiation-induced murine thymic lymphomas [22], direct evidence has not yet been reported.

To identify the mode of *Pten* inactivation in hematopoietic malignancies, we systematically analyzed the status of *Pten* alleles and Pten expression at the RNA and protein levels in 23 radiation-induced thymic lymphomas developed in B6C3F1 mice; downstream activation of Akt was also analyzed. These analyses revealed that biallelic structural abnormality of *Pten*, but not epigenetic silencing, plays a significant role in radiation-induced lymphomagenesis.

2. Materials and methods

2.1. Tumor induction

The induction of thymic lymphomas was carried out as described [23], with minor modifications. In brief, female B6C3F1 mice were exposed weekly to 2.0 Gy whole-body X-ray radiation for four consecutive weeks starting at four weeks of age. Mice were observed daily until moribund and were then sacrificed under ether anesthesia. All experiments with mice were conducted according to the legal regulations in Japan and were in compliance with the guidelines for the care of laboratory animals of the National Institute of Radiological Sciences.

2.2. LOH analysis

For LOH analysis, genomic DNA was amplified by PCR using the following polymorphic markers: *D19Mit59*, *D19Mit46*, *D19Mit19*, *D19Mit53* and *D19Mit34* (see Supplementary Table 1). To determine LOH at the *Pten* locus, the microsatellite sequence was searched using the UCSC Genome Bioinformatics database (http://genome.ucsc.edu/). A repetitive region within intron 2, which contained fragment length polymorphism between C57BL/6 and C3H/HeJ mice, was identified. PCR products amplified from genomic DNA of C57BL/6 and C3H/HeJ mice that contained this region were sequenced, and the polymorphism was confirmed. The primer sequences and the conditions for each PCR reaction are described in Supplementary Table 1. PCR products were resolved using a capillary electrophoresis system HAD-GT12 Genetic Analyzer (eGene Inc., Irvine, CA, USA) or by 3% NuSieve agarose (3:1) gel electrophoresis (FMC, Rockland, MA, USA).

2.3. RT-PCR analysis

Total RNA was extracted from tumor tissues using the acid guanidinium thiocyanate–phenol-chloroform method [24], and the cDNA was reverse transcribed using 10 μg total RNA, Moloney murine leukemia virus reverse transcriptase (Toyobo Co., Ltd., Osaka, Japan), and random hexamers (Takara Bio) according to the manufacturer's recommendations. The primer sequences and the conditions for each PCR reaction are described in Supplementary Table 1. PCR products were resolved by 2% agarose gel electrophoresis and analyzed using a Luminescent image analyzer LAS-3000 (Fujifilm, Tokyo, Japan). PCR products were directly sequenced using a Big Dye Terminator v3.1 (Applied Biosystems, Foster City, CA, USA) and an ABI PRISM 3100 Genetic Analyzer (Applied Biosystems) or sequenced after TA cloning using a TOPO TA cloning kit (Invitrogen Co., Carlsbad, CA, USA).

2.4. Bisulfite sequencing analysis

Genomic DNA (1.0 μg) was subjected to bisulfite modification using a CpGenome DNA modification kit, No. S7820 (Chemicon, Temecula, CA, USA), according to the manufacturer's instructions. Bisulfite-modified DNA (40 ng/μl) was then subjected to PCR amplification using primers specific for methylated CpG cytosines as described in Supplementary Table 1. PCR products were sequenced after TA cloning.

2.5. Western blot analysis

Thymic lymphoma cells and normal thymocytes were dissolved in cell lysis buffer (Cell Signaling Technology Inc., Danvers, MA, USA) containing phenylmethanesulfonyl fluoride. Proteins were denatured by heating at 100 °C for 5 min in sample buffer containing SDS, and then lysates (20 μg) were separated by 10% SDS-PAGE and transferred to a PVDF membrane (Millipore Co., Billerica, MA, USA). Anti-Pten, anti-Akt, anti-phospho-Akt (Ser473) and anti-beta-actin (Santa Cruz Biotechnology Inc., Santa Cruz, CA, USA) were used as primary antibodies. Horseradish peroxidase-conjugated anti-rabbit (Cell Signaling Technology) or anti-goat (Santa Cruz Biotechnology) IgG was used as secondary antibody. Signals were developed using ECL plus Western Blotting Detection Reagents (GE Healthcare, Little Chalfont, Buckinghamshire, UK) and analyzed using the LAS-3000 luminescent image analyzer (Fujifilm).

2.6. Array-CGH analysis

We designed and used an Agilent 8 × 15k-formatted mouse custom array-CGH microarray (#020410; Agilent Technologies, Santa Clara, CA, USA), which consisted of about 15,000 oligonucleotide probes, including 1499 for the genomic region covering the *Pten* locus on chromosome 19 (about 430 kbp). Fluorescence labeling of DNA, microarray hybridization and post-hybridization washing were carried out according to the manufacturer's protocol (version 5) for genomic DNA analysis using oligonucleotide array-CGH. Scanning was performed using an Agilent microarray scanner (G2565BA). Signal intensities were measured and evaluated using Agilent

Feature Extraction software v9-5-35 and CGH analytics software v3-5-14, respectively. The microarray data reported in this article have been deposited in the Gene Expression Ominibus (GEO) database, www.ncbi.nlm.nih.gov/geo (accession no. GSE17751).

2.7. Quantitative real-time RT-PCR

Quantitative real-time RT-PCR analysis of miR-19a and miR-21 was performed using a TaqMan MicroRNA assay kit (Applied Biosystems) according to manufacturer's recommendations. Quantitative PCR amplification of cDNAs was performed using a Mx3000P real-time PCR system (Stratagene, La Jolla, CA, USA) and TaqMan Universal PCR Master Mix (Applied Biosystems). Data were normalized to the levels of the small nucleolar RNAs 202 and 234. Each reaction was performed in triplicate. Data were analyzed with MxPro software, version 4.10 (Stratagene).

3. Results

3.1. LOH analysis

Mouse *Pten* encodes a protein product predicted to have 403 amino acid residues and is located at 24.5 cM on chromosome 19. We analyzed LOH using five independent microsatellite simple-sequence-length polymorphism makers on chromosome 19. LOH at the *Pten* locus was also examined using a microsatellite marker within intron 2, which distinguished the polymorphism between C57BL/6 and C3H/HeJ mice. LOH around the *Pten* locus was identified in seven lymphomas (TL8, 11, 12, 14, 19, 20 and 21) (Fig. 1). The LOH frequency (30%; 7 of 23 lymphomas) was roughly consistent with previous studies examining radiation-induced thymic lymphomas in various F1 hybrid mouse strains [22,23,25].

3.2. Expression of Pten mRNA and protein

We examined the expression of *Pten* transcripts by reverse transcriptase (RT)-PCR analysis using three sets of primers (Fig. 2). Altered expression of *Pten* mRNA was observed in 5 of 23 lymphomas (TL5, 8, 11, 14 and 20). TL5 had an additional but faint PCR product that was larger than the predicted product when amplified using primers Ex2F and Ex7R. For TL8, RT-PCR products generated using any primer combination were faint or undetectable. LOH at the *Pten* locus in TL8 indicated that one *Pten* allele remained. Thus the absence of *Pten* transcripts suggested the transcriptional silencing at the *Pten* promoter region in the remaining allele. Using the Ex1F-7R primer pair, TL11 generated one RT-PCR product of the predicted length and three longer RT-PCR products; TL14 generated a faint, short RT-PCR product in addition to a product of the predicted length. TL20 generated a faint product when primers Ex1F and Ex7R were used, but a substantial amount of product was generated using either of the remaining two sets of primers, suggesting that a 5′ portion of exon 1 was missing.

3.3. Sequencing of bisulfite-modified DNA

Because our data for TL8 implicated transcriptional silencing of *Pten* (Figs. 1 and 2), we analyzed the DNA methylation pat-

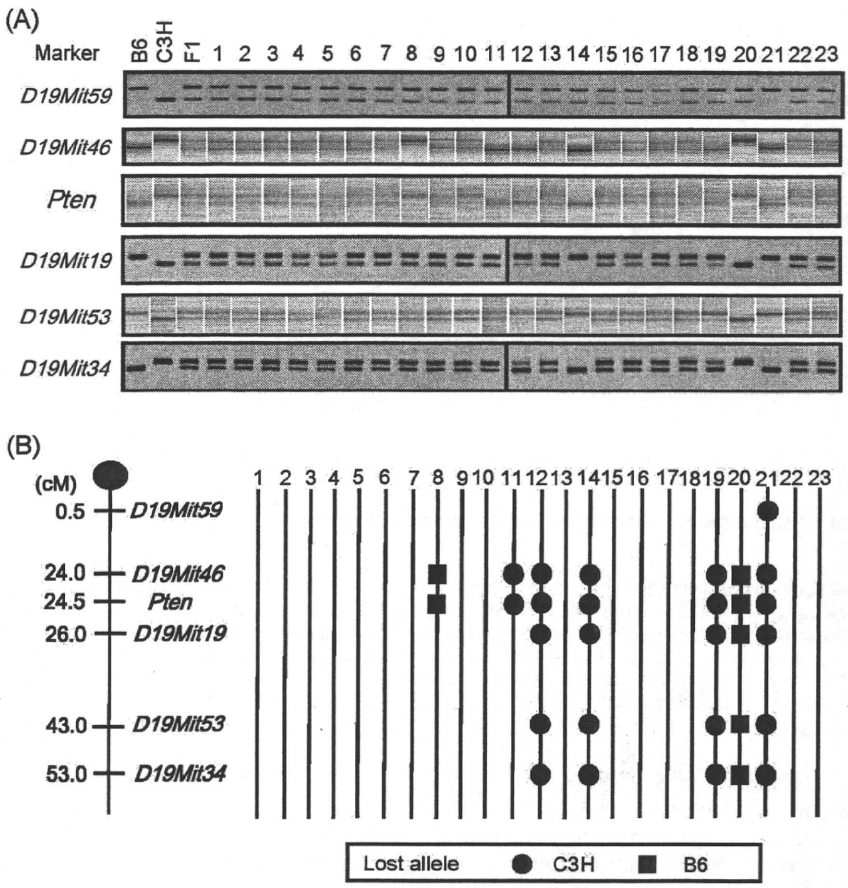

Fig. 1. LOH analysis of chromosome 19 in 23 radiation-induced thymic lymphomas. (A) The first three lanes represent control DNA samples from the maternal C57BL/6 strain (B6), the paternal C3H/HeJ strain (C3H), and the B6C3F1 hybrid (F1), respectively. Numbers above the remaining lanes reflect the tumor identification numbers. PCR amplification of genomic DNA was performed using the indicated polymorphic marker primer pair followed by electrophoretic analysis of amplification products. (B) Schematic diagram of LOH on chromosome 19 in each lymphoma. Lymphoma identification numbers are indicated at top. Polymorphic markers are shown to the right of the chromosome schematic, and marker positions indicating distances (cM) from the centromere are shown at left. The *Pten* marker is located between exons 2 and 3. Absence of a circle or square indicates the retention of heterozygosity.

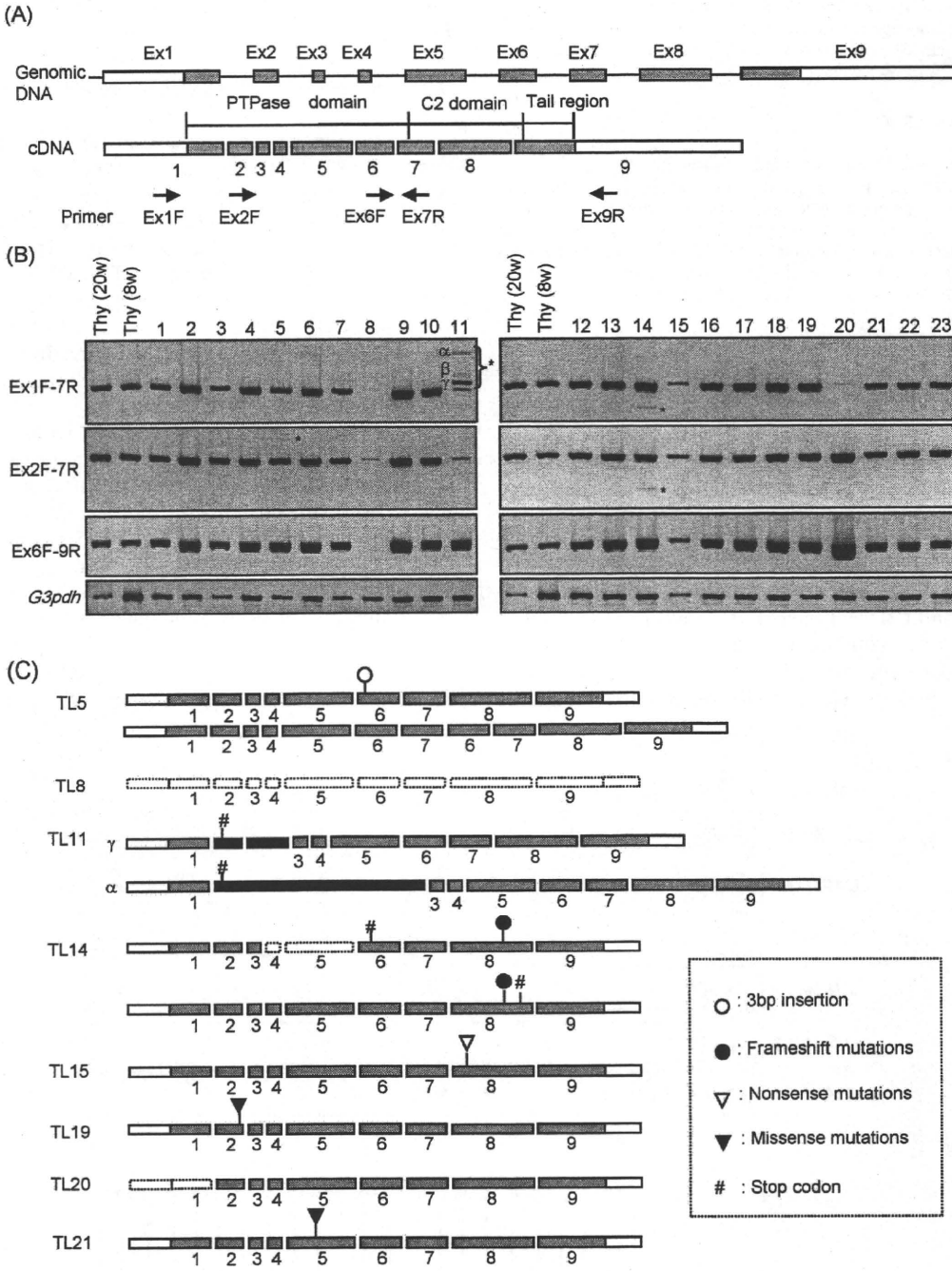

Fig. 2. Alteration of *Pten* in radiation-induced thymic lymphomas. (A) Schematic representation of *Pten*. Shading indicates the *Pten* coding regions. RT-PCR amplification primers and their annealing locations are indicated by arrows. Ex, exon; PTPase, phosphotyrosine protein phosphatase. (B) RT-PCR analysis of *Pten* using the primer pairs indicated at left and genomic DNA isolated from thymocytes (Thy) of 20- or 8-week-old mice (control lanes 1 and 2, respectively), or from the lymphoma indicated at top, was performed and reaction products were subjected to 2% agarose gel electrophoresis. *G3pdh* was used as a control for RT-PCR amplification and as a loading control. Asterisks indicate RT-PCR products longer or shorter than the expected size. (C) Schematic representation of aberrant *Pten* transcripts. Black bars in TL11 indicate inserted intronic sequences. #, Positions of newly generated in-frame stop codons that possibly cause immature translation.

terns in the 5′ (upstream) region of *Pten* (Supplementary Fig. 1A, indicated as P1) in all lymphomas; this region corresponds to the promoter of human *PTEN* that was shown to be aberrantly methylated in T-cell ALLs [26]. However, no aberrant methylation was detected (Supplementary Fig. 1B). Although the CpG sites at positions -39 and -40 relative to the transcriptional start site were both methylated in most of the lymphomas, these CpG sites were also frequently methylated in normal thymocytes. For TL8, we analyzed an additional *Pten* region (Supplementary Fig. 1A, indicated as P2) in which hypermethylation has been suggested to be associated with a lack of *PTEN* expression in non-small cell lung cancer [27]. However, we again did not detect aberrant methylation (Supplementary Fig. 1C). Thus, the absence of *Pten* transcripts likely resulted from a mechanism other than silencing by DNA methylation.

3.4. Sequence analysis of Pten transcripts

Next, we determined the sequence of the RT-PCR products from all lymphomas including those products that were longer or shorter than predicted in TL5, 11 and 14 (Fig. 2C). In TL5, the longer

PCR product generated using the Ex2F-7R primer pair contained duplicated exons 6 and 7. The product of predicted length had an insertion of 3 bp, which encoded an amino acid change from Ser170 to Met and Cys. Because the normal *Pten* sequence was not observed, TL5 may contain biallelic *Pten* mutations. TL11 had one RT-PCR product of predicted length and three longer products when amplified using the Ex1F-7R primer pair. The most predominant longer fragment generated from TL11 (Fig. 2B, indicated as γ) contained two large nucleotide insertions of 88 and 122 bp within intron 1 that generated a stop codon, together with a deletion of exon 2. The least predominant longer fragment generated from TL11 (Fig. 2B, indicated as α) contained a 1078-bp insertion in intron 1 and a deletion of exon 2, generating a stop codon. Sequencing of the TL11 PCR product β could not be achieved. The faint product of predicted length had no mutations but may have been derived from contamination of the tumor sample with healthy cells. In TL14, the predominant product of predicted length generated using the Ex6F-9R primer pair had a frameshift mutation due to a 1-bp insertion (962insA) in the poly(A)6 stretch in exon 8, creating a downstream stop codon. The faint/short PCR product of TL14, generated using either Ex1F-7R or Ex2F-7R primer pairs, had both the frameshift mutation and loss of exons 4 and 5, the latter of which generated a stop codon at residue 264. TL15 had an allele with a *Pten* nonsense mutation owing to a substitution (base 862G to T) in addition to a wild-type allele. TL19 had a *Pten* missense mutation owing to a substitution (base 158T to C), resulting in V53A. TL19 generated both mutated and wild-type PCR products, coincident with incomplete allelic LOH in TL19 (Fig. 1A). TL20 expressed only a single *Pten* transcript that lacked exon 1. TL21 had a missense mutation (base 364A to T) in *Pten*, resulting in I122F.

Overall, *Pten* transcripts in radiation-induced lymphomas had a variety of genetic lesions including missense mutations (TL19 and 21), nonsense mutations (TL15), 1- and 3-base insertions (TL14 and 5, respectively), partial intron insertions (TL11), exon duplication (TL5), exon deletion (TL11, 14, 20), and null expression (TL8). Although these mutations are very complicated, they were in good agreement with previous reports demonstrating that missense mutations occur in the Pten phosphatase domain whereas nonsense and frameshift mutations, resulting in protein truncation, occur in the C2 domain of Pten. In total, seven of eight lymphomas carrying a *Pten* mutation (88%) contained biallelic alterations.

3.5. Array-based comparative genomic hybridization (array-CGH) analysis of genomic DNA from TL8, 11 and 20

In order to know the reason for the absence or aberrant transcription of *Pten* in TL8, 11 and 20 (Fig. 2), we analyzed genomic structures around the *Pten* locus in TL8, 11 and 20 using array-CGH, which was designed for intensive analysis of the *Pten* locus. As shown in Fig. 3, the array-CGH profiles suggested partial homozygous deletions (<30 kbp) in the *Pten* locus in these lymphomas, which were positioned within the regions of hemizygous deletion in TL8 and 11. A region of homozygous deletion (~24 kbp) in TL8 occurred in the 5′ (upstream) region of *Pten*, encompassing both the putative promoter region and the transcription initiation site; this may account for the *Pten* silencing observed in TL8 (Fig. 2). Two RT-PCR products from TL11 had a deletion of exon 2 together with one or two insertion(s) of a partial sequence of intron 1 (Supplementary Fig. 2). Array-CGH indicated that TL11 had a homozygous deletion that extended 1 kbp downstream of exon 1 into the 5′ flanking region of exon 2, suggesting that the abnormal transcripts were generated by aberrant splice-site selection likely resulting from the absence of correct splice sites at the intron 1/exon 2 boundary. Array-CGH analysis of TL20 also revealed homozygous deletion of genomic regions (~4 kbp), including both the putative promoter region and the *Pten* transcription initiation site. RT-PCR analysis

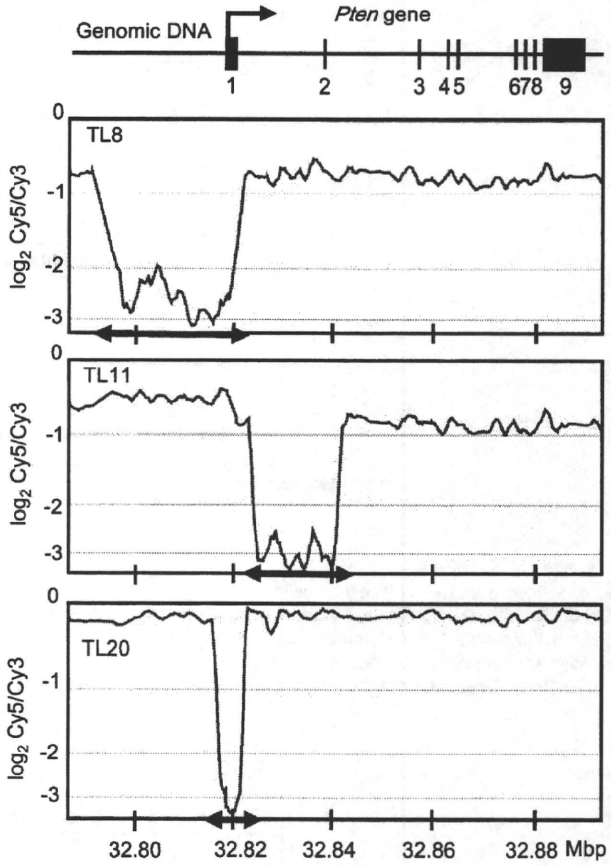

Fig. 3. Array-CGH analysis reveals homozygous focal deletions in three radiation-induced thymic lymphomas (TL8, 11 and 20). Schematic of *Pten* (top), in which shaded bars represent exons aligned to the genomic positions on chromosome 19 indicated along the *x*-axis in the array-CGH profiles below the schematic. Moving averages of the normalized $\log_2$ Cy5/Cy3 ratio, calculated based on 10 data points, are plotted in the array-CGH profiles. Arrows on the *x*-axis correspond to genomic regions amplified by PCR and sequenced to identify breakpoints.

indicated the presence of a *Pten* transcript, however, suggesting that the ectopic transcription was initiated at a cryptic promoter in TL20.

To explore the mechanism responsible for these deletions, genomic regions containing the breakpoints (indicated by the *x*-axis arrows in Fig. 3) were amplified by PCR and sequenced (Fig. 4), which identified nucleotide insertions at the breakpoint junctions in TL8 and 11. In TL11, a pair of recombination signal sequence-like sequences, composed of heptamer- and nonamer-like motifs separated by non-conserved spacers of 12 or 23 bp, were located between but immediately adjacent to the breakpoints, suggesting that illegitimate V(D)J recombination gave rise to the deletion. In contrast, a 0.8-kb templated nucleotide sequence was inserted in the TL20 deletion region. Overlaps of 1 or 2 nucleotides at both breakpoints of the two junctions were identified, suggesting that microhomology-mediated rearrangements might have led to the deletion.

3.6. Loss of Pten and downstream activation of Akt

Pten protein expression varied in the lymphomas we examined (Fig. 5). To determine whether decreased expression correlated with loss of Pten function, we analyzed the degree of Ser473 phosphorylation in Akt (Fig. 5). Pten was not expressed in lymphomas TL8, 11, 14 and 20, consistent with the aberrant stop codon and genomic deletions in the *Pten* promoter region. Pten expression level correlated inversely with phosphorylation of Akt. Lymphomas

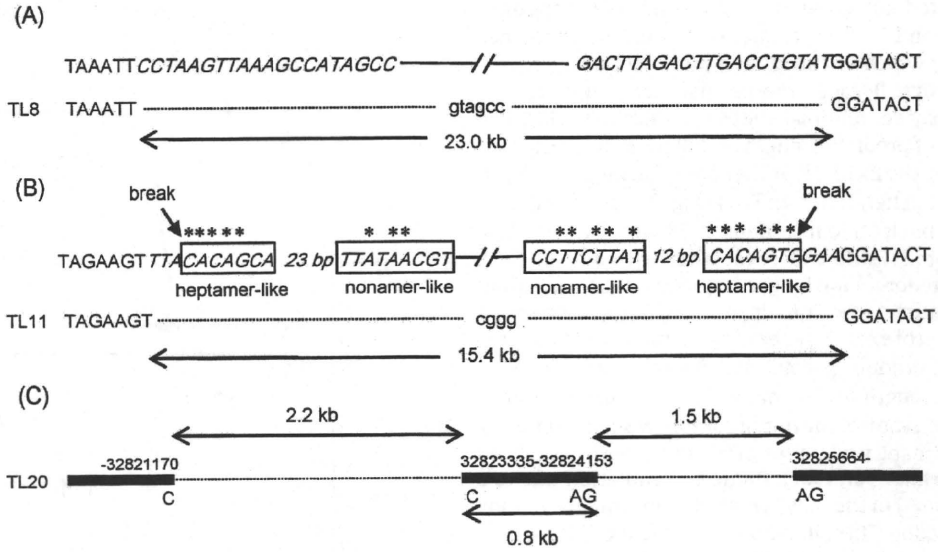

Fig. 4. Sequence analysis of *Pten* focal deletion breakpoints. Schematic diagram representing sequence analysis of focal deletion breakpoints in *Pten* in TL8 (A), TL11 (B) and TL20 (C) lymphomas. Dotted lines indicate deleted genomic regions, and the deleted wild-type sequence is shown in italics in (A and B). Boxes indicate heptamer-like or nonamer-like motifs, and nucleotides marked with asterisks are identical to the canonical heptamer or nonamer sequences. Arrows indicate the sites of Rag-mediated DNA breakage. Lowercase letters indicate nucleotide insertions. Black bars indicate the positions (mm8 assembly) of the retained DNA ends. The uppercase letters below the line in (C) indicate the sequences used to locate microhomology at both ends of each deletion.

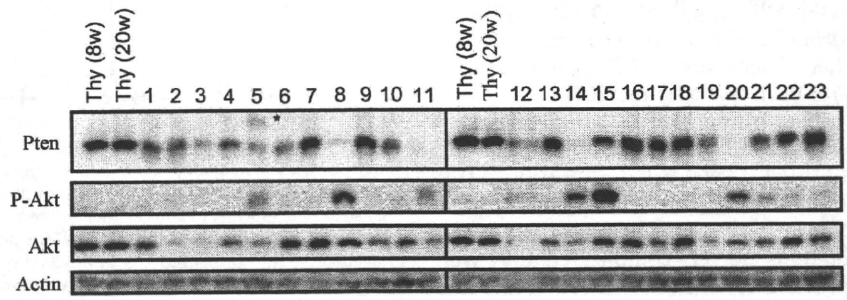

Fig. 5. Analysis of Pten expression and Akt phosphorylation in radiation-induced thymic lymphomas. Western blot analysis of lysates from 23 radiation-induced T-cell lymphomas was performed using antibodies to the proteins indicated at left. Lanes 1 and 2, control thymocytes (Thy) of 8- and 20-week-old mice, respectively. Actin was analyzed as loading control. Asterisk indicates polypeptide with larger mass than expected.

TL5, 19 and 21 expressed mutant Pten containing amino acid substitutions in the phosphatase domain. In TL5 and 21, Akt phosphorylation was weakly observed, suggesting dysfunction of Pten. In TL19, Akt phosphorylation was not observed. The lack of phosphorylation of Akt might have resulted from decreased levels of Akt protein. In TL3 and 12, in which the Pten expression level was low, Akt phosphorylation was not observed owing to negligible expression of Akt protein. In contrast, Akt was highly phosphorylated in TL15, which expressed wild-type Pten. It is possible that other factors that regulate the phosphorylation of Akt, such as PI3K and Ship, may activate Akt independently of Pten [28,29].

3.7. *Levels of Pten-targeting microRNAs do not correlate with Pten protein levels in lymphomas*

Lymphomas TL3, 6 and 12 contained low levels of Pten protein, although neither a decrease in the amounts of RT-PCR product nor genetic aberrations were observed. Recent reports have revealed the involvement of microRNAs in downregulation of Pten expression [13,14,30–33]. We therefore examined whether certain microRNAs contributed to post-transcriptional downregulation of the expression of Pten. For all lymphomas with sufficient available RNA, expression levels of the well-studied *Pten*-targeting microRNAs miR-19a and miR-21 were analyzed using real-time RT-PCR (Supplementary Fig. 3). Expression of miR-19a was almost constant among all lymphomas and was similar to the expression levels in normal thymocytes from 20-week-old mice. Some lymphomas exhibited relatively high miR-21 expression, but there was no significant inverse correlation between miR-21 expression level and Pten protein level.

4. Discussion

In our present study of radiation-induced thymic lymphomas, *Pten* inactivation occurred with a frequency of 30% (7 of 23 lymphomas) and was caused by a variety of biallelic structural abnormalities including base substitutions, long and short (1 and 3 bp) insertions, duplication, and deletions (Table 1). Epigenetic silencing was not observed.

Frequent LOH around the *PTEN* locus has been reported in human leukemias (20% frequency) and lymphomas (23% frequency) [34,35]. *PTEN* alterations, however, have only been sporadically detected in hematopoietic neoplasms [36–42]. In contrast, aberrant DNA methylation in the *PTEN* promoter region has been detected at a frequency of 20% in T-cell ALLs and at a frequency of 18% in B-cell ALLs [26], suggesting that epigenetic silencing is a dominant mechanism of *PTEN* inactivation in hematopoietic neoplasms. Santos et al. [22] has suggested that

Pten in radiation-induced mouse thymic lymphomas also undergoes epigenetic silencing in C57BL/6J and BALB/c F1 hybrid mice. In our present study, however, no aberrant DNA methylation was detected in CpG islands located in the 5′ (upstream) region of *Pten*. Thus, epigenetic silencing does not play a major role in *Pten* loss in radiation-induced thymic lymphomas in B6C3F1 mice. Mao et al. [61] also reported that *Pten* does not undergo methylation-mediated transcriptional silencing in $p53^{+/-}$and $p53^{-/-}$mice. The reason for these discrepancies is not clear, although different mice strains may exhibit distinct patterns of CpG island methylation. Indeed, it has been reported that patterns of CpG island methylation in T-cell lymphomas are driven by the genetic configuration of tumor cells [43]. Santos et al. [22] reported that intragenic mutations do not occur in any genes on chromosome 19, including *Pten*, in C57BL/6J and BALB/c F1 hybrid mice. In contrast, our data indicated frequent intragenic mutations of *Pten* in C57BL/6J and C3H/HeJ F1 hybrid mice, as was suggestive of the influence of the host genetic background on the mutation spectrum. We previously demonstrated strain-based differences between C57BL/6 and C3H mice with respect to genomic alterations of *Kras* and genome-wide copy numbers in thymic lymphomas [44,45].

We have shown that LOH of *Pten* occurred at a frequency of about 30% (7 of 23 lymphomas) and that 8 lymphomas contained complex *Pten* structural abnormalities. Most of the available information regarding the mutation spectrum of *PTEN* has been derived mainly from epithelial cancers such as endometrial carcinomas, glioblastomas, prostate carcinomas, and others [6,7]. In these cases missense, nonsense and frameshift mutations predominate; missense mutations have been found to cluster in exons 5 and 6, encoding the PTEN phosphatase domain, and nonsense and frameshift mutations cluster in the poly $(A)_6$ stretches and in exons 7 and 8, encoding the C2 domain [6]. Comparison of mutations has shown that *PTEN* mutations in tumors depend on tissue type. Endometrial carcinomas predominantly contain frameshift mutations (>60% frequency), whereas glioblastomas contain fewer frameshift mutations but more missense mutations (61% frequency). Recently, *PTEN* frameshift mutations were found to cluster exclusively in exon 7 in human T-cell ALLs [29]. On the other hand, hemizygous *PTEN* deletions have been reported in 39% of prostatic adenocarcinomas, and homozygous *PTEN* deletion has been observed in 5% of prostate tumors [46]. Of note, hemizygous *PTEN* deletion is usually accompanied by an interstitial microdeletion.

In this study, we detected focal homozygous deletions at *Pten* in 13% of lymphomas (3/23; TL8, 11 and 20), all of which resulted in dearth of Pten protein. In two lymphomas (TL8 and 11), homozygous deletions were positioned within hemizygous deletions, possibly resulting from independent deletions occurring in both alleles in these lymphomas. On the other hand, TL20 had a homozygous deletion without adjacent hemizygous deletions. The observation that TL20 contained distally extending continuous LOH on chromosome 19 suggests that this homozygous deletion might have been caused by sequential events, in which one small deletion within the *Pten* locus was followed by subsequent mitotic recombination. Notably, microdeletions have been reported in several key tumor-related genes, such as *IKZF1*, *PAX5* and *CDKN2A*, in human ALLs [47–51] and in *Nocth1* and *Bcl11b* in murine thymic lymphomas [52,53]. The sequence at the deletion breakpoint strongly suggests that these deletions were generated by illegitimate V(D)J recombination and microhomology-mediated rearrangement [49,52–54]. Homozygous *PTEN* deletions were recently identified in 4% of human primary childhood T-cell ALLs [29].

A previous study on T-cell lymphomas developed in chromosomally unstable *Terc*-, *Atm*- and *Trp53*-null mice also reported frequent homozygous deletions at the *Pten* locus [39]. In addition, recent reports on breast cancers [55] and medulloblastomas [56] demonstrated that *Pten* was selectively targeted in a background of defective homologous recombination repair of DNA double-strand breaks (DSBs). Importantly, radiation is a genotoxic stress that increases the frequency of DSBs and stimulates V(D)J rearrangements at cryptic recombination signal sequences [57]. Therefore, radiation-induced DNA DSBs may facilitate hemi- and homozygous deletions of the *Pten* locus.

The two-hit model posits that both copies of a tumor suppressor gene must be inactivated before cancer can develop [58]. Some tumor suppressor genes, however, are inactivated solely by hemizygous loss, indicating the involvement of haploinsufficiency. Several lines of evidence suggest that *Pten* is such a haploinsufficient tumor suppressor gene, at least in epithelial cancers such as prostate cancer [59,60]. A study of radiation-induced lymphomas from *Trp53* heterozygous and/or null mice suggested that *Pten* is a haploinsufficient tumor suppressor gene and that *Pten* haploinsufficiency is a common characteristic of radiation-induced lymphoma development [61]. It is unclear whether *Pten* is inactivated in a bi- or mono-allelic manner in thymic lymphomas of wild-type mice. In the present study, biallelic *Pten* inactivation occurred in seven of eight lymphomas. Although complete loss of *Pten* resulted in increased phosphorylation of Akt, lymphomas with decreased *Pten* expression or monoallelic inactivation (TL15) did not always exhibit increased Akt phosphorylation. Together with the frequent biallelic point mutations and microdeletions observed at the *Pten* locus, these findings suggest that decreased *Pten* dosage alone is not sufficient for activation of the PI3K/Akt signaling pathway during radiation-induced lymphomagenesis. Manifestation of *Pten* haploinsufficiency may require other genetic or epigenetic aberrations. It has been suggested that in tumors of defined tissue origin and genetic background, *Pten* functions in a haploinsufficient manner, but that for others both alleles need to be inactivated [62].

Conflicts of interest

The authors declare that there are no conflicts of interest.

Acknowledgements

The authors thank Dr. K. Ariyoshi, Mr. Y. Kodama and Ms. Y. Nishimura for their valuable technical tutorship and discussion. We also express our gratitude to all laboratory members for their encouragement throughout this work, and to the Laboratory Animal Science Section in National Institute of Radiological Sciences for animal management. This work was supported by institutional funds from the National Institute of Radiological Sciences (Chiba, Japan). This work was also supported financially by a Grant-in-Aid from the Ministry of Education, Culture, Sports, Sciences, and Technology of Japan (to Y.S.) and by a grant from the Long-Range Research Initiative of the Japan Chemical Industry Association (to Y.S. and S.K.).

Appendix A. Supplementary data

Supplementary data associated with this article can be found, in the online version, at doi:10.1016/j.mrfmmm.2009.12.011.

References

[1] V. Stambolic, A. Suzuki, J.L. de la Pompa, G.M. Brothers, C. Mirtsos, T. Sasaki, J. Ruland, J.M. Penninger, D.P. Siderovski, T.W. Mak, Negative regulation of PKB/Akt-dependent cell survival by the tumor suppressor PTEN, Cell 95 (1998) 29–39.

[2] H. Sun, R. Lesche, D.M. Li, J. Liliental, H. Zhang, J. Gao, N. Gavrilova, B. Mueller, X. Liu, H. Wu, PTEN modulates cell cycle progression and cell survival by regulating phosphatidylinositol 3,4,5,-trisphosphate and Akt/protein kinase B signaling pathway, Proc. Natl. Acad. Sci. U.S.A. 96 (1999) 6199–6204.

[3] P.L. Dahia, R.C. Aguiar, J. Alberta, J.B. Kum, S. Caron, H. Sill, D.J. Marsh, J. Ritz, A. Freedman, C. Stiles, C. Eng, PTEN is inversely correlated with the cell survival factor Akt/PKB and is inactivated via multiple mechanisms in haematological malignancies, Hum. Mol. Genet. 8 (1999) 185–193.
[4] G.C. Fillmore, Q. Wang, M.J. Carey, C.H. Kim, K.S. Elenitoba-Johnson, M.S. Lim, Expression of Akt (protein kinase B) and its isoforms in malignant lymphomas, Leuk. Lymphoma 46 (2005) 1765–1773.
[5] W.H. Shen, A.S. Balajee, J. Wang, H. Wu, C. Eng, P.P. Pandolfi, Y. Yin, Essential role for nuclear PTEN in maintaining chromosomal integrity, Cell 128 (2007) 157–170.
[6] I.U. Ali, L.M. Schriml, M. Dean, Mutational spectra of PTEN/MMAC1 gene: a tumor suppressor with lipid phosphatase activity, J. Natl. Cancer Inst. 91 (1999) 1922–1932.
[7] D. Bonneau, M. Longy, Mutations of the human PTEN gene, Hum. Mutat. 16 (2000) 109–122.
[8] Y. Yin, W.H. Shen, PTEN: a new guardian of the genome, Oncogene 27 (2008) 5443–5453.
[9] L.C. Cantley, B.G. Neel, New insights into tumor suppression: PTEN suppresses tumor formation by restraining the phosphoinositide 3-kinase/AKT pathway, Proc. Natl. Acad. Sci. U.S.A. 96 (1999) 4240–4245.
[10] D. Liaw, D.J. Marsh, J. Li, P.L. Dahia, S.I. Wang, Z. Zheng, S. Bose, K.M. Call, H.C. Tsou, M. Peacocke, C. Eng, R. Parsons, Germline mutations of the PTEN gene in Cowden disease, an inherited breast and thyroid cancer syndrome, Nat. Genet. 16 (1997) 64–67.
[11] J.M. Garcia, J. Silva, C. Pena, V. Garcia, R. Rodriguez, M.A. Cruz, B. Cantos, M. Provencio, P. Espana, F. Bonilla, Promoter methylation of the PTEN gene is a common molecular change in breast cancer, Genes Chromosomes Cancer 41 (2004) 117–124.
[12] Y.H. Kang, H.S. Lee, W.H. Kim, Promoter methylation and silencing of PTEN in gastric carcinoma, Lab. Invest. 82 (2002) 285–291.
[13] F. Meng, R. Henson, H. Wehbe-Janek, K. Ghoshal, S.T. Jacob, T. Patel, MicroRNA-21 regulates expression of the PTEN tumor suppressor gene in human hepatocellular cancer, Gastroenterology 133 (2007) 647–658.
[14] H. Yang, W. Kong, L. He, J.J. Zhao, J.D. O'Donnell, J. Wang, R.M. Wenham, D. Coppola, P.A. Kruk, S.V. Nicosia, J.Q. Cheng, MicroRNA expression profiling in human ovarian cancer: miR-214 induces cell survival and cisplatin resistance by targeting PTEN, Cancer Res. 68 (2008) 425–433.
[15] K. Sircar, M. Yoshimoto, F.A. Monzon, I.H. Koumakpayi, R.L. Katz, A. Khanna, K. Alvarez, G. Chen, A.D. Darnel, A.G. Aprikian, F. Saad, T.A. Bismar, J.A. Squire, PTEN genomic deletion is associated with p-Akt and AR signalling in poorer outcome, hormone refractory prostate cancer, J. Pathol. 218 (2009) 505–513.
[16] Y. Shang, S. Kakinuma, Y. Amasaki, M. Nishimura, Y. Kobayashi, Y. Shimada, Aberrant activation of interleukin-9 receptor and downstream Stat3/5 in primary T-cell lymphomas in vivo in susceptible B6 and resistant C3H mice, In Vivo 22 (2008) 713–720.
[17] M. Malumbres, I. Perez de Castro, J. Santos, B. Melendez, R. Mangues, M. Serrano, A. Pellicer, J. Fernandez-Piqueras, Inactivation of the cyclin-dependent kinase inhibitor p15INK4b by deletion and de novo methylation with independence of p16INK4a alterations in murine primary T-cell lymphomas, Oncogene 14 (1997) 1361–1370.
[18] S. Kakinuma, M. Nishimura, S. Sasanuma, K. Mita, G. Suzuki, Y. Katsura, T. Sado, Y. Shimada, Spectrum of Znfn1a1 (Ikaros) inactivation and its association with loss of heterozygosity in radiogenic T-cell lymphomas in susceptible B6C3F1 mice, Radiat. Res. 157 (2002) 331–340.
[19] H. Okano, Y. Saito, T. Miyazawa, T. Shinbo, D. Chou, S. Kosugi, Y. Takahashi, S. Odani, O. Niwa, R. Kominami, Homozygous deletions and point mutations of the Ikaros gene in gamma-ray-induced mouse thymic lymphomas, Oncogene 18 (1999) 6677–6683.
[20] H. Tsuji, H. Ishii-Ohba, H. Ukai, T. Katsube, T. Ogiu, Radiation-induced deletions in the 5′ end region of Notch1 lead to the formation of truncated proteins and are involved in the development of mouse thymic lymphomas, Carcinogenesis 24 (2003) 1257–1268.
[21] D.P. Hong, K. Kubo, N. Tsugawa, N. Mori, S. Umesako, C.W. Song, M. Okumoto, Generation of large homozygous chromosomal segments by mitotic recombination during lymphomagenesis in F1 hybrid mice, J. Radiat. Res. (Tokyo) 43 (2002) 187–194.
[22] J. Santos, M. Herranz, M. Fernandez, C. Vaquero, P. Lopez, J. Fernandez-Piqueras, Evidence of a possible epigenetic inactivation mechanism operating on a region of mouse chromosome 19 in gamma-radiation-induced thymic lymphomas, Oncogene 20 (2001) 2186–2189.
[23] Y. Shimada, M. Nishimura, S. Kakinuma, M. Okumoto, T. Shiroishi, K.H. Clifton, S. Wakana, Radiation-associated loss of heterozygosity at the Znfn1a1 (Ikaros) locus on chromosome 11 in murine thymic lymphomas, Radiat. Res. 154 (2000) 293–300.
[24] P. Chomczynski, N. Sacchi, Single-step method of RNA isolation by acid guanidinium thiocyanate–phenol-chloroform extraction, Anal. Biochem. 162 (1987) 156–159.
[25] H. Ohi, Y. Mishima, K. Kamimura, M. Maruyama, K. Sasai, R. Kominami, Multistep lymphomagenesis deduced from DNA changes in thymic lymphomas and atrophic thymuses at various times after gamma-irradiation, Oncogene 26 (2007) 5280–5289.
[26] J. Roman-Gomez, A. Jimenez-Velasco, X. Agirre, F. Prosper, A. Heiniger, A. Torres, Lack of CpG island methylator phenotype defines a clinical subtype of T-cell acute lymphoblastic leukemia associated with good prognosis, J. Clin. Oncol. 23 (2005) 7043–7049.
[27] J.C. Soria, H.Y. Lee, J.I. Lee, L. Wang, J.P. Issa, B.L. Kemp, D.D. Liu, J.M. Kurie, L. Mao, F.R. Khuri, Lack of PTEN expression in non-small cell lung cancer could be related to promoter methylation, Clin. Cancer Res. 8 (2002) 1178–1184.
[28] J.M. Luo, Z.L. Liu, H.L. Hao, F.X. Wang, Z.R. Dong, R. Ohno, Mutation analysis of SHIP gene in acute leukemia, Zhongguo Shi Yan Xue Ye Xue Za Zhi 12 (2004) 420–426.
[29] A. Gutierrez, T. Sanda, R. Grebliunaite, A. Carracedo, L. Salmena, Y. Ahn, S. Dahlberg, D. Neuberg, L.A. Moreau, S.S. Winter, R. Larson, J. Zhang, A. Protopopov, L. Chin, P.P. Pandolfi, L.B. Silverman, S.P. Hunger, S.E. Sallan, A.T. Look, High frequency of PTEN, PI3K and AKT abnormalities in T cell acute lymphoblastic leukemia, Blood (2009).
[30] G.L. Huang, X.H. Zhang, G.L. Guo, K.T. Huang, K.Y. Yang, X.Q. Hu, Expression of microRNA-21 in invasive ductal carcinoma of the breast and its association with phosphatase and tensin homolog deleted from chromosome expression and clinicopathologic features, Zhonghua Yi Xue Za Zhi 88 (2008) 2833–2837.
[31] J.T. Huse, C. Brennan, D. Hambardzumyan, B. Wee, J. Pena, S.H. Rouhanifard, C. Sohn-Lee, C. le Sage, R. Agami, T. Tuschl, E.C. Holland, The PTEN-regulating microRNA miR-26a is amplified in high-grade glioma and facilitates gliomagenesis in vivo, Genes Dev. 23 (2009) 1327–1337.
[32] M.G. Pezzolesi, P. Platzer, K.A. Waite, C. Eng, Differential expression of PTEN-targeting microRNAs miR-19a and miR-21 in Cowden syndrome, Am. J. Hum. Genet. 82 (2008) 1141–1149.
[33] S. Roy, S. Khanna, S.R. Hussain, S. Biswas, A. Azad, C. Rink, S. Gnyawali, S. Shilo, G.J. Nuovo, C.K. Sen, MicroRNA expression in response to murine myocardial infarction: miR-21 regulates fibroblast metalloprotease-2 via phosphatase and tensin homologue, Cardiovasc. Res. 82 (2009) 21–29.
[34] H. Chang, X.Y. Qi, J. Claudio, L. Zhuang, B. Patterson, A.K. Stewart, Analysis of PTEN deletions and mutations in multiple myeloma, Leuk. Res. 30 (2006) 262–265.
[35] J.J. Scarisbrick, A.J. Woolford, R. Russell-Jones, S.J. Whittaker, Loss of heterozygosity on 10q and microsatellite instability in advanced stages of primary cutaneous T-cell lymphoma and possible association with homozygous deletion of PTEN, Blood 95 (2000) 2937–2942.
[36] A. Aggerholm, K. Gronbaek, P. Guldberg, P. Hokland, Mutational analysis of the tumour suppressor gene MMAC1/PTEN in malignant myeloid disorders, Eur. J. Haematol. 65 (2000) 109–113.
[37] K. Gronbaek, J. Zeuthen, P. Guldberg, E. Ralfkiaer, K. Hou-Jensen, Alterations of the MMAC1/PTEN gene in lymphoid malignancies, Blood 91 (1998) 4388–4390.
[38] G. Lenz, G.W. Wright, N.C. Emre, H. Kohlhammer, S.S. Dave, R.E. Davis, S. Carty, L.T. Lam, A.L. Shaffer, W. Xiao, J. Powell, A. Rosenwald, G. Ott, H.K. Muller-Hermelink, R.D. Gascoyne, J.M. Connors, E. Campo, E.S. Jaffe, J. Delabie, E.B. Smeland, L.M. Rimsza, R.I. Fisher, D.D. Weisenburger, W.C. Chan, L.M. Staudt, Molecular subtypes of diffuse large B-cell lymphoma arise by distinct genetic pathways, Proc. Natl. Acad. Sci. U.S.A. 105 (2008) 13520–13525.
[39] R.S. Maser, B. Choudhury, P.J. Campbell, B. Feng, K.K. Wong, A. Protopopov, J. O'Neil, A. Gutierrez, E. Ivanova, I. Perna, E. Lin, V. Mani, S. Jiang, K. McNamara, S. Zaghlul, S. Edkins, C. Stevens, C. Brennan, E.S. Martin, R. Wiedemeyer, O. Kabbarah, C. Nogueira, G. Histen, J. Aster, M. Mansour, V. Duke, L. Foroni, A.K. Fielding, A.H. Goldstone, J.M. Rowe, Y.A. Wang, A.T. Look, M.R. Stratton, L. Chin, P.A. Futreal, R.A. DePinho, Chromosomally unstable mouse tumours have genomic alterations similar to diverse human cancers, Nature 447 (2007) 966–971.
[40] Y. Nakahara, H. Nagai, T. Kinoshita, T. Uchida, S. Hatano, T. Murate, H. Saito, Mutational analysis of the PTEN/MMAC1 gene in non-Hodgkin's lymphoma, Leukemia 12 (1998) 1277–1280.
[41] T. Palomero, M.L. Sulis, M. Cortina, P.J. Real, K. Barnes, M. Ciofani, E. Caparros, J. Buteau, K. Brown, S.L. Perkins, G. Bhagat, A.M. Agarwal, G. Basso, M. Castillo, S. Nagase, C. Cordon-Cardo, R. Parsons, J.C. Zuniga-Pflucker, M. Dominguez, A.A. Ferrando, Mutational loss of PTEN induces resistance to NOTCH1 inhibition in T-cell leukemia, Nat. Med. 13 (2007) 1203–1210.
[42] A. Sakai, C. Thieblemont, A. Wellmann, E.S. Jaffe, M. Raffeld, PTEN gene alterations in lymphoid neoplasms, Blood 92 (1998) 3410–3415.
[43] R. Opavsky, S.H. Wang, P. Trikha, A. Raval, Y. Huang, Y.Z. Wu, B. Rodriguez, B. Keller, S. Liyanarachchi, G. Wei, R.V. Davuluri, M. Weinstein, D. Felsher, M. Ostrowski, G. Leone, C. Plass, CpG island methylation in a mouse model of lymphoma is driven by the genetic configuration of tumor cells, PLoS Genet. 3 (2007) 1757–1769.
[44] Y. Shimada, M. Nishimura, S. Kakinuma, T. Ogiu, H. Fujimoto, A. Kubo, J. Nagai, K. Kobayash, K. Tano, S. Yoshinaga, K.K. Bhakat, Genetic susceptibility to thymic lymphomas and K-ras gene mutation in mice after exposure to X-rays and N-ethyl-N-nitrosourea, Int. J. Radiat. Biol. 79 (2003) 423–430.
[45] T. Takabatake, S. Kakinuma, T. Hirouchi, M.M. Nakamura, K. Fujikawa, M. Nishimura, Y. Oghiso, Y. Shimada, K. Tanaka, Analysis of changes in DNA copy number in radiation-induced thymic lymphomas of susceptible C57BL/6, resistant C3H and hybrid F1 Mice, Radiat. Res. 169 (2008) 426–436.
[46] M. Yoshimoto, I.W. Cunha, R.A. Coudry, F.P. Fonseca, C.H. Torres, F.A. Soares, J.A. Squire, FISH analysis of 107 prostate cancers shows that PTEN genomic deletion is associated with poor clinical outcome, Br. J. Cancer 97 (2007) 678–685.
[47] N. Kawamata, S. Ogawa, M. Zimmermann, M. Kato, M. Sanada, K. Hemminki, G. Yamatomo, Y. Nannya, R. Koehler, T. Flohr, C.W. Miller, J. Harbott, W.D. Ludwig, M. Stanulla, M. Schrappe, C.R. Bartram, H.P. Koeffler, Molecular allelokaryotyping of pediatric acute lymphoblastic leukemias by high-resolution single nucleotide polymorphism oligonucleotide genomic microarray, Blood 111 (2008) 776–784.

[48] C.G. Mullighan, S. Goorha, I. Radtke, C.B. Miller, E. Coustan-Smith, J.D. Dalton, K. Girtman, S. Mathew, J. Ma, S.B. Pounds, X. Su, C.H. Pui, M.V. Relling, W.E. Evans, S.A. Shurtleff, J.R. Downing, Genome-wide analysis of genetic alterations in acute lymphoblastic leukaemia, Nature 446 (2007) 758–764.
[49] C.G. Mullighan, C.B. Miller, I. Radtke, L.A. Phillips, J. Dalton, J. Ma, D. White, T.P. Hughes, M.M. Le Beau, C.H. Pui, M.V. Relling, S.A. Shurtleff, J.R. Downing, BCR-ABL1 lymphoblastic leukaemia is characterized by the deletion of Ikaros, Nature 453 (2008) 110–114.
[50] K. Paulsson, J.B. Cazier, F. Macdougall, J. Stevens, I. Stasevich, N. Vrcelj, T. Chaplin, D.M. Lillington, T.A. Lister, B.D. Young, Microdeletions are a general feature of adult and adolescent acute lymphoblastic leukemia: unexpected similarities with pediatric disease, Proc. Natl. Acad. Sci. U.S.A. 105 (2008) 6708–6713.
[51] A. Usvasalo, S. Savola, R. Raty, K. Vettenranta, A. Harila-Saari, P. Koistinen, E.R. Savolainen, E. Elonen, U.M. Saarinen-Pihkala, S. Knuutila, CDKN2A deletions in acute lymphoblastic leukemia of adolescents and young adults: an array CGH study, Leuk. Res. 32 (2008) 1228–1235.
[52] J. Sakata, J. Inoue, H. Ohi, H. Kosugi-Okano, Y. Mishima, K. Hatakeyama, O. Niwa, R. Kominami, Involvement of V(D)J recombinase in the generation of intragenic deletions in the Rit1/Bcl11b tumor suppressor gene in gamma-ray-induced thymic lymphomas and in normal thymus of the mouse, Carcinogenesis 25 (2004) 1069–1075.
[53] H. Tsuji, H. Ishii-Ohba, T. Katsube, H. Ukai, S. Aizawa, M. Doi, K. Hioki, T. Ogiu, Involvement of illegitimate V(D)J recombination or microhomology-mediated nonhomologous end-joining in the formation of intragenic deletions of the Notch1 gene in mouse thymic lymphomas, Cancer Res. 64 (2004) 8882–8890.
[54] F. Novara, S. Beri, M.E. Bernardo, R. Bellazzi, A. Malovini, R. Ciccone, A.M. Cometa, F. Locatelli, R. Giorda, O. Zuffardi, Different molecular mechanisms causing 9p21 deletions in acute lymphoblastic leukemia of childhood, Hum. Genet. (2009).
[55] L.H. Saal, S.K. Gruvberger-Saal, C. Persson, K. Lovgren, M. Jumppanen, J. Staaf, G. Jonsson, M.M. Pires, M. Maurer, K. Holm, S. Koujak, S. Subramaniyam, J. Vallon-Christersson, H. Olsson, T. Su, L. Memeo, T. Ludwig, S.P. Ethier, M. Krogh, M. Szabolcs, V.V. Murty, J. Isola, H. Hibshoosh, R. Parsons, A. Borg, Recurrent gross mutations of the PTEN tumor suppressor gene in breast cancers with deficient DSB repair, Nat. Genet. 40 (2008) 102–107.
[56] P.O. Frappart, Y. Lee, H.R. Russell, N. Chalhoub, Y.D. Wang, K.E. Orii, J. Zhao, N. Kondo, S.J. Baker, P.J. McKinnon, Recurrent genomic alterations characterize medulloblastoma arising from DNA double-strand break repair deficiency, Proc. Natl. Acad. Sci. U.S.A. 106 (2009) 1880–1885.
[57] R.L. Pinsonneault, P.M. Vacek, J.P. O'Neill, B.A. Finette, Induction of V(D)J-mediated recombination of an extrachromosomal substrate following exposure to DNA-damaging agents, Environ. Mol. Mutagen. 48 (2007) 440–450.
[58] A.G. Knudson Jr., Mutation and cancer: statistical study of retinoblastoma, Proc. Natl. Acad. Sci. U.S.A. 68 (1971) 820–823.
[59] A. Di Cristofano, M. De Acetis, A. Koff, C. Cordon-Cardo, P.P. Pandolfi, Pten and p27KIP1 cooperate in prostate cancer tumor suppression in the mouse, Nat. Genet. 27 (2001) 222–224.
[60] L.C. Trotman, M. Niki, Z.A. Dotan, J.A. Koutcher, A. Di Cristofano, A. Xiao, A.S. Khoo, P. Roy-Burman, N.M. Greenberg, T. Van Dyke, C. Cordon-Cardo, P.P. Pandolfi, Pten dose dictates cancer progression in the prostate, PLoS Biol. 1 (2003) E59.
[61] J.H. Mao, D. Wu, J. Perez-Losada, H. Nagase, R. DelRosario, A. Balmain, Genetic interactions between Pten and p53 in radiation-induced lymphoma development, Oncogene 22 (2003) 8379–8385.
[62] M. Santarosa, A. Ashworth, Haploinsufficiency for tumour suppressor genes: when you don't need to go all the way, Biochim. Biophys. Acta 1654 (2004) 105–122.

RADIATION RESEARCH 173, 310–318 (2010)
0033-7587/10 $15.00

DOI: 10.1667/RR1905.1

Unique Characteristics of Radiation-Induced Apoptosis in the Postnatally Developing Small Intestine and Colon of Mice

T. Miyoshi-Imamura,[a,b] S. Kakinuma,[b] M. Kaminishi,[b] M. Okamoto,[b] T. Takabatake,[b] Y. Nishimura,[b] T. Imaoka,[b] M. Nishimura,[b] K. Murakami-Murofushi[a] and Y. Shimada[b,1]

[a] *Genetic Counseling Program, Graduate School of Humanities and Sciences, Ochanomizu University, 2-1-1 Otsuka, Bunkyo-ku, Tokyo, 112-8610, Japan; and* [b] *Experimental Radiology for Children's Health Research Group, National Institute of Radiological Sciences, 4-9-1 Anagawa, Inage-ku, Chiba, 263-8555, Japan*

Miyoshi-Imamura, T., Kakinuma, S., Kaminishi, M., Okamoto, M., Takabatake, T., Nishimura, Y., Imaoka, T., Nishimura, M., Murakami-Murofushi, K. and Shimada, Y. Unique Characteristics of Radiation-Induced Apoptosis in the Postnatally Developing Small Intestine and Colon of Mice. *Radiat. Res.* 173, 310–318 (2010).

We examined the response of the developing mouse intestine to X radiation using neonates (1 day postpartum), infants (2 weeks postpartum) and adults (7 weeks postpartum). Irradiated adult small intestinal crypts displayed two waves of apoptosis. The first wave peaked at 3 h and was followed by a broad wave with a peak persisting from 24 to 48 h. p53 was expressed during the first wave but not the second wave. For the infant small intestine, the intensity of the first wave was approximately half that of the adult wave, and for the colon the intensity was even smaller. In neonates, apoptosis was delayed, peaking at 6 h for small intestinal crypts and at 24 h for colonic crypts. Although no apoptosis occurred at 3 h postirradiation in neonates, p53 was present in both the small intestine and colon, owing at least in part to the inability of p53 to increase the level of Noxa, a p53-dependent pro-apoptosis protein, suggesting a discontinuity in the p53-Noxa-caspase pathway in neonates. By contrast, the induction of p21, a pro-survival protein, was greater in neonatal cells than in adult cells. Thus it appears that the developing and adult intestine mount distinct apoptotic responses to radiation.

INTRODUCTION

Fetuses and young children should not be considered simply as small adults but rather as a unique cohort when assessing the health risks of exposure to environmental carcinogens such as ionizing radiation. Members of this cohort appear to be especially vulnerable to radiation because their organs grow more rapidly and are less differentiated than those of adults. Radiation damage to the tissues has been shown to depend on the degree of cell proliferation and the extent of differentiation. A century ago, Bergonie and Tribondeau stated that "tissues appear to be more radiosensitive if their cells have a greater proliferative capacity, divide more rapidly, and are less-well differentiated" (*1*). The cells of the developing cerebral cortex and the developing kidney are highly susceptible to radiation-induced apoptosis—a sensitivity that is lost after differentiation (*2, 3*). Irradiated hematopoietic and mammary stem cells of weanling mice have been shown to be more severely damaged than those of adult mice (*4, 5*). Exposure of infant mice to 1.5 Gy of radiation depresses their levels of hematopoietic stem cells for a long time thereafter (*6*).

Apoptosis is a form of programmed cell death, i.e., a genetically controlled self-destruction process, occurring during developmental tissue morphogenesis and adult tissue homeostasis (*7*). Apoptosis can be induced by exposure to exogenous DNA-damaging agents including ionizing radiation. Intestinal tract organs of wild-type and genetically engineered adult mice have been used extensively as *in vivo* systems to assess the effects of radiation-induced apoptosis (*8*). The properties that have been monitored include dose response, temporal patterns of apoptosis, spatial distribution of susceptible cells in crypts, differential susceptibilities of small intestinal and colonic epithelial cells and of regions within the colon, and p53, p21 and Bcl-2 activities (*9–24*). However, similar studies using the intestines of neonates and infants have not been undertaken. Therefore, in this study we characterized the features of radiation-induced apoptosis in the postnatally developing small intestine and colon of C57BL/6J mice and compared these features to those of identically treated adult mice. We found that the postnatally developing intestine is more resistant to radiation-induced apoptosis than with the adult intestine, which could be ascribed in part to an apparent inability to completely carry out the post-p53-mediated pathway to apoptosis.

[1] Address for correspondence: Experimental Radiology for Children's Health Research Group, National Institute of Radiological Sciences, 4-9-1 Anagawa, Inage-ku, Chiba, 263-8555, Japan; e-mail: y_shimad@nirs.go.jp.

MATERIALS AND METHODS

Mice

Female C57BL/6J mice were purchased from Charles River Laboratories (Kanagawa, Japan). All mice were exposed to a 12-h dark-light cycle, a temperature of 23 ± 2°C, and 50 ± 10% humidity. They were fed a standard laboratory diet (MB-1; Funabashi Farm Co., Ltd., Chiba, Japan) and given water *ad libitum*. The experimental protocol was reviewed and approved by our institution's animal use committee.

Irradiation of Mice

Irradiation was performed using a Pantak X-ray generator (Pantak Ltd., East Haven, CT). One-day-old (neonate), 2-week-old (infant), and 7-week-old (adult) mice were whole-body irradiated with 2 Gy at a dose rate of 0.7 Gy/min (200 kVp, 20 mA, with a filter composed of 0.5-mm-thick copper and aluminum plates). Subsequently, mice were killed humanely at 0 (unirradiated), 3, 6, 12, 24, 48 and 72 h after irradiation.

Pathology

Unirradiated and irradiated mice were killed after ether anesthesia. Then their small intestines and colons were removed, rinsed in ice-cold phosphate-buffered saline, and fixed quickly in 10% neutral-buffered formalin for about 12 h. Each organ was divided into proximal, middle and distal sections. All samples were embedded in paraffin, sectioned transversely (3–4 μm thick), and stained with hematoxylin and eosin.

Immunohistochemistry

Immunostaining of paraffin-embedded samples followed standard procedures. To retrieve antigens using the primary antibodies [rabbit polyclonal anti-active caspase-3 (1:750, AF835; R&D Systems, Abingdon, UK); rabbit polyclonal anti-p53 (1:500, NCL-p53-CM5; Novocastral Laboratories Ltd., Newcastle, UK); rabbit polyclonal anti-Noxa (1:100, LS-B184/6830; LifeSpan Biosciences, Seattle, WA); rabbit polyclonal anti-p21 (1:500, sc397; Santa Cruz Biotechnology Inc., Santa Cruz, CA); and rat polyclonal anti-Ki-67 (1:100, M7249; DAKO Carpinteria, CA)], the tissue sections in 10 m*M* sodium citrate, pH 6.0, were heated at 120°C for 20 min. After the primary antibodies were washed away, sections were incubated with a peroxidase-conjugated secondary antibody [Histofine® Simple Stain MAX PO(R) or Histofine® Simple Stain MAX PO(Rat); Nichirei Biosciences, Tokyo, Japan]. Peroxidase activity was visualized by first staining with 3,3′-diaminobenzidine (Simple Stain DAB Solution, Nichirei Biosciences, Tokyo, Japan) and then counterstaining with hematoxylin.

Scoring the Numbers and Types of Small Intestinal and Colonic Crypts

The crypt number was defined as the total number of crypts per circumference and was determined by counting the number from crypts found in two to three transverse sections of three mice. For the purpose of identifying the small intestinal crypts, the presence of Paneth cells defined the crypts of mature mice, and clear epithelial invaginations into the mucosa defined the crypts of neonatal and infant mice. We counted a crypt undergoing cleavage, i.e., "crypt fission" or "branching", as two crypts.

Morphologically, apoptosis was defined as the presence of an apoptotic body. This definition correlated well with one that relied on immunohistochemical staining of active caspase 3 (*17*). To quantify the extent of apoptosis, we used two different scoring systems: scoring the number of crypts (as a percentage) containing one or more active caspase 3-positive cells per circumference, and scoring the mean number of apoptotic cells per crypt. However, the extent of apoptosis in the small intestine of 1-day-old mice was scored as the mean number of active caspase 3-positive cells per circumference in the transverse sections, because crypts had not yet formed. The same scoring systems were used to quantify the number of p53-positive crypts (as a percentage) and the mean number of p53-positive cells per crypt. All scoring was performed without knowing whether the mice had been irradiated.

Statistical Analysis

Data are expressed as means ± SEM. Each experiment used three mice. The Student's *t* test ($P < 0.05$) was used to determine whether experimental values differed significantly between two groups.

RESULTS

Normal Development of Crypts in the Small Intestine and Colon

We first examined the development of intestinal crypts, focusing on morphology and the number of crypts. Plots of the number of crypts present as a function of time and examples of crypt cells expressing Ki-67, reflecting active phases of the cell cycle, are shown in Fig. 1. Supplementary Fig. S1 shows micrographs that document the developmental changes occurring in the anatomical structures of normal small intestinal and colonic crypts between 1 day and 7 weeks postpartum.

1. Small intestine

In the small intestine at 1 day postpartum, invaginating clusters of epithelial cells could be found, but crypts had not yet formed. Morphologically apparent crypts were identified in the proximal region between 4 days and 1 week postpartum and were found next in the middle region and finally in the distal region (Fig. 1A). Then the size and number of crypts increased rapidly (with occasional crypt fission) until 4 weeks postpartum when morphologically mature crypts appeared (Fig. 1A and Supplementary Fig. S1). The number of crypts was nearly constant thereafter (Fig. 1A). Goblet cells were observed 1 day postpartum in the distal region, and Paneth cells, located at the bottom of crypts, developed 1 to 2 weeks postpartum (Supplementary Fig. S1).

At 1 day postpartum, Ki-67 expression was observed in the nuclei of clustered epithelial cells, presumably indicating crypt formation. At 2 weeks postpartum, Ki-67 staining was uniform within a crypt, i.e., was independent of cell position. By 7 weeks postpartum, cells in the proliferative zone (above cell position 4) were most heavily stained (Fig. 1C), as has been reported previously (*18, 19*).

2. Colon

Crypt-like structures were observed at 1 day postpartum (Fig. 1B and Supplementary Fig. S1). Crypt

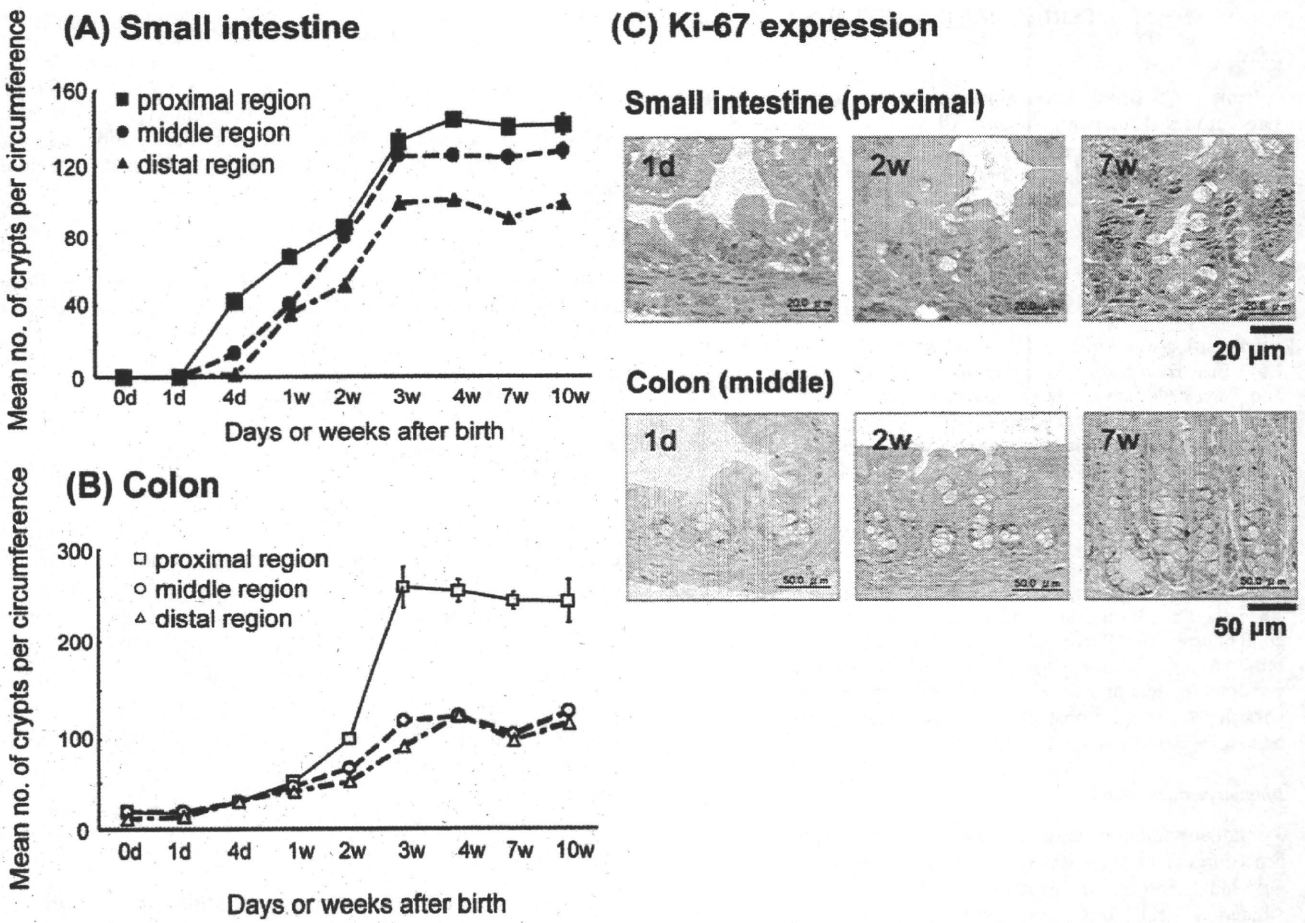

FIG. 1. Developmental changes in the mean number of crypts per circumference for the proximal, middle and distal regions of the small intestine (panel A) and the colon (panel B). Data are reported as means ± SEM. Each experiment used three mice. Panel C: Photomicrographs of Ki-67-stained sections of the small intestine and colon of 1-day-old (1d), 2-week-old (2w) and 7-week-old (7w) mice.

number and size increased with age until 3 to 4 weeks postpartum and were accompanied by frequent crypt fission. Morphologically mature crypts appeared 4 weeks postpartum. The proximal region contained approximately twice as many crypts as did the middle and distal regions (Fig. 1B). Goblet cells developed during the fetal stage (data not shown), which was much earlier than in the small intestine (Supplementary Fig. S1). Ki-67-positive cells were located in the basal one-half to two-thirds of the crypt regardless of age, which was distinctly different from what was seen in the small intestine (Fig. 1C).

Radiation-Induced Apoptosis in Small Intestinal and Colonic Crypts

We next analyzed radiation-induced apoptosis in mice exposed to 2 Gy at 1 day, 2 weeks and 7 weeks postpartum as representatives of neonates with immature or undifferentiated crypts, infants with active proliferative crypts, and adults with a steady number of crypts maintained, respectively (Fig. 1). The dose of 2 Gy was selected based on evidence that the apoptosis in response to ionizing radiation saturates at 1 Gy (*25*). Apoptotic cells were defined as those containing apoptotic bodies and strongly staining for active caspase 3 (*17*). The age and region dependences of the apoptotic response in these mice are shown in Figs. 2, 3 and 4.

1. Small intestine

For mice irradiated at 7 weeks postpartum, apoptosis of crypt cells occurred in two waves (Figs. 2A and 3A). The first wave peaked 3 h after irradiation, as reported previously (*17*), followed by a rapid decrease. The percentage of apoptotic crypts in the first wave was greater than 75% in all regions of the small intestine (Figs. 2A and 4A), and the average number of apoptotic cells was two per crypt (Fig. 3A). The second wave arose thereafter, and its peak level persisted until 48 h. From 10% to 20% of the crypts exhibited apoptosis (Fig. 2A). There were no clear differences among the temporal patterns of the proximal, middle and distal regions (Figs. 2A and 3A). The second apoptotic wave might

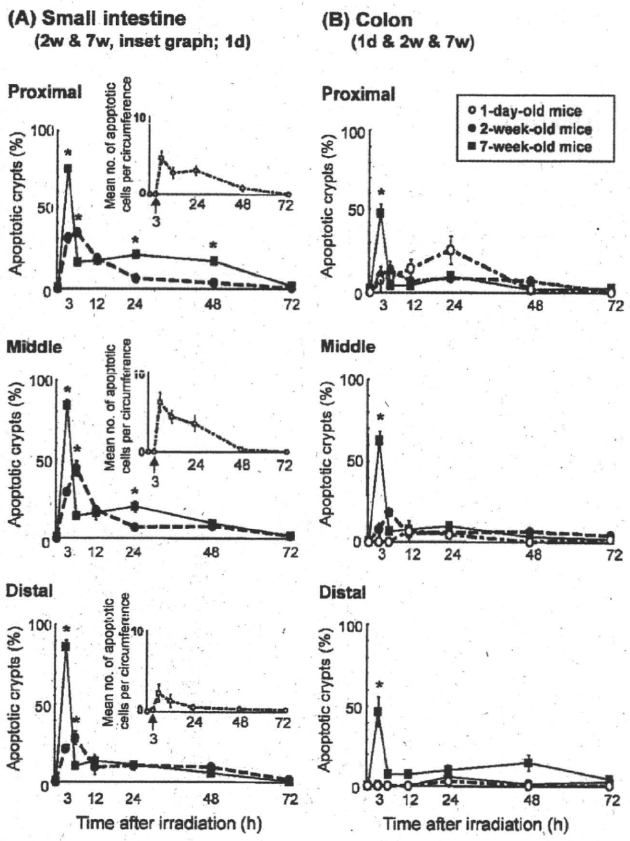

FIG. 2. Percentage of apoptotic crypts as a function of time for the proximal, middle and distal regions of the small intestine (panel A) and the colon (panel B) of mice irradiated at 1 day (1d), 2 weeks (2w) and 7 weeks (7w) postpartum. The inset is a plot of the mean number of apoptotic cells per circumference for 1-day-old irradiated mice. All data are reported as means ± SEM. Each experiment used three mice. For the data points for 2- and 7-week-old mice labeled with an asterisk (*), $P < 0.05$.

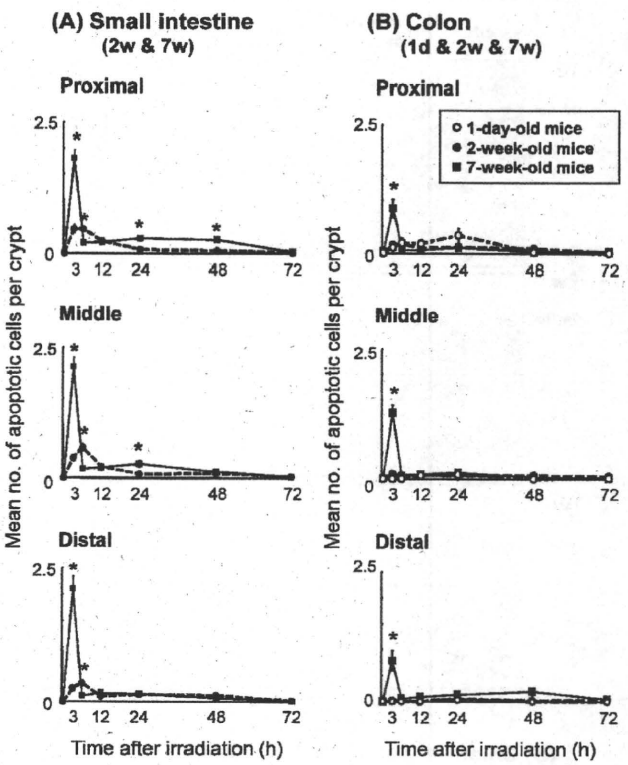

FIG. 3. Mean number of apoptotic cells per crypt as a function of time for the proximal, middle and distal regions of the small intestine of mice irradiated 2 weeks (2w) and 7 weeks (7w) postpartum (panel A) and the colon of mice irradiated 1 day (1d), 2 weeks (2w), and 7 weeks (7w) postpartum (panel B). All data are reported as means ± SEM. Each experiment used three mice. For the data points for 2- and 7-week-old mice labeled with an asterisk (*), $P < 0.05$.

have been the result of a delayed mitotic crisis involving cells that escaped apoptosis during the first wave but then reached the G_2/M checkpoint (*12*).

Compared with the results for 7-week-old mice, the percentage of apoptotic small intestinal crypts in 2-week-old mice at 3 h postirradiation was significantly lower (approximately 20% to 30%; $P < 0.05$; Figs. 2A and 4A). The peak of the first wave occurred 6 h postirradiation, and the average numbers of apoptotic cells per crypt were 0.4, 0.6 and 0.3 for the proximal, middle and distal regions, respectively (Fig. 3A). Only the crypts of the distal region were involved in the second wave of apoptosis (Fig. 2A).

Because no small intestinal crypts were found before the first postpartum day, for the tissues of 1-day-old mice, we used the mean number of apoptotic cells per circumference as a measure of apoptosis. We did not observe any apoptotic cells 3 h after irradiation, instead finding that the maximum apoptosis index occurred at 6 h and persisted until 24 h (Figs. 2A inset and 4A). The mean numbers of apoptotic cells per circumference at 6 h postirradiation were 4.8, 6.2 and 2.3 for the proximal, middle and distal regions, respectively (Fig. 2A insets). At 1 day postpartum, there were approximately 300 to 400 epithelial cells per circumference, which means that approximately 1% of the epithelial cells were very radiosensitive.

2. *Colon*

For 7-week-old mice, the apoptotic response peaked sharply 3 h postirradiation and was followed by a smaller broad response between 24 and 48 h (Figs. 2B, 3B and 4B). Fewer apoptotic cells were found in colonic crypts than in small intestinal crypts (Fig. 3B), as reported previously (*20*). The percentage of apoptotic crypts for the first wave ranged from 47% to 63%, and the average was slightly more than 0.8 apoptotic cell per crypt (Fig. 2B). Conversely, the apoptosis index of colonic crypts of mice irradiated 2 weeks postpartum was much lower, and the maximum values observed for crypts in the proximal and middle regions occurred at 6 h (Fig. 2B). No apoptotic cells were found in the distal region until 12 h postirradiation (Fig. 2B). Colonic cells